Thesis for the degree of doctor of philosophy

Excited States in Negative Ions

Johan Rohlén

UNIVERSITY OF GOTHENBURG

Department of Physics
University of Gothenburg
Gothenburg 2014

ISBN 978-91-628-9058-2
E-Published at http://hdl.handle.net/2077/35580

Typeset using LaTeX
Figures created using Matlab and InkScape

Department of Physics
University of Gothenburg
SE-412 96 Gothenburg, Sweden
Phone: +46 (0)31 786 0000

Printed by Ale Tryckteam
Gothenburg, Sweden 2014

Excited States in Negative Ions
Johan Rohlén
Department of Physics
University of Gothenburg
SE-412 96 Gothenburg, Sweden

Abstract

This thesis covers experimental studies of atomic negative ions with the main goal of increasing our fundamental understanding of these fragile quantum systems. Comparisons of measurements and calculations have been used to increase our understanding of these highly correlated, yet simple, systems. All the described studies in this thesis have investigated the photodetachment process, i.e. when a photon removes an electron from a negative ion. The measurements were mainly performed using a collinear laser-ion beam setup at the Gothenburg University Negative Ion Laser LAboratory (GUNILLA).

Novel threshold behavior was observed in studies of photodetachment of K^-, Cs^- and Na^- to highly excited states of the residual atom that has a large and negative polarizability. The cross section of this process was seen to be greatly suppressed just above threshold. In contrast, if the residual atom is left in a state with a large and positive polarizability a rapidly rising onset in the cross section was observed. The two behaviours are attributed to the fact that the detached electron either travels in a strongly repulsive or strongly attractive potential. These potentials are similar to those found in β-decay and are an excellent example of the generality of physics. A semi-classical model was developed in order to explain the novel threshold behavior.

In the studies on K^- and Cs^-, resonances due to doubly excited states were observed to modulate the cross sections in several photodetachment channels. In the case of K^- three known and two unknown resonances were observed below the $7\,^2P$ threshold. For Cs^-, a rich spectrum of overlapping resonances was observed below the $10\,^2P$ threshold. A new resonance parametrization was developed in order to handle the overlapping resonances.

A new field ionization setup has been developed in order to investigate the photodetachment process in greater detail. This apparatus will enable three new types of measurements: partial cross sections to very highly excited states approaching the double detachment limit; branching ratios to Rydberg states in the same energy range; and near threshold cross sections for the fundamentally interesting double photodetachment process. Initial experiments on the photodetachment of Cs^- leading to highly excited states of Cs are presented in this thesis.

In addition to the work at GUNILLA, an experiment has been performed on La^- at the Department of Physics at Denison University using a crossed laser-ion beams setup. Twelve optically allowed transitions between bound states of opposite parity in La^- were observed. One such transition has properties that could make it a candidate for the first laser cooling of a negative ion. If successful, laser cooled negative ions could be used in a proposed process of sympathetic cooling of anti-protons in an effort to enhance the production of anti-hydrogen.

Contents

Appended Publications

This thesis is based on the work presented in the following six papers, appended to the thesis, which are referred to by capital roman numerals in the text.

I Experimental Studies of Partial Photodetachment Cross Sections in K^- Below the K(7 ^{2}P) Threshold
A. O. Lindahl, J. Rohlén, H. Hultgren, I. Yu. Kiyan, D. J. Pegg, C. W. Walter, and D. Hanstorp
Physical Review A, **85**:033415, 2012

II Observation of Thresholds and Overlapping Resonances Below the 10 $^2P_{1/2}$ and $^2P_{3/2}$ Thresholds in the Photodetachment of Cs^-
A. O. Lindahl, J. Rohlén, H. Hultgren, D. J. Pegg, C. W. Walter, and D. Hanstorp
Physical Review A, **88**:053410, 2013

III Threshold Photodetachment in a Repulsive Potential
A. O. Lindahl, J. Rohlén, H. Hultgren, I. Yu. Kiyan, D. J. Pegg, C. W. Walter, and D. Hanstorp
Physical Review Letters, **108**:033004, 2012

IV Threshold Behaviour in Photodetachment into a Final State With Large Negative Polarizability
J. Rohlén, A. O. Lindahl, H. Hultgren, R. D. Thomas, D. J. Pegg, and D. Hanstorp
Submitted to Europhysics Letters

V A Field Ionizer for Photodetachment Studies of Negative Ions
J. Rohlén, T. Leopold, J. Welander, R. D. Thomas, D. J. Pegg, and D. Hanstorp
Manuscript

VI A Promising Candidate for Laser Cooling of a Negative Ion: Observations of Bound-Bound Transitions in La^-
C. W. Walter, N. D. Gibson, D. J. Matyas, C. Crocker, K. A. Dungan, B. R. Matola, and J. Rohlén
Submitted to Physical Review Letters

Additional Publications

I have during my time as a Ph.D. student published six additional papers. They are, however, slightly outside the scope of this thesis and are therefore not included.

1. Acceleration and rotation in a pendulum ride, measured using an iPhone 4
   A.-M. Pendrill and J. Rohlén
   Physics Education, **46**:676, 2011

2. Reassessment of ^{182}Hf AMS Measurements at VERA
   O. Forstner, H. Gnaser, R. Golser, D. Hanstorp, M. Martschini, A. Priller, J. Rohlén, P. Steier, C. Vockenhuber, and A. Wallner
   Nuclear Instruments and Methods in Physics Research Section B: Beam Interactions with Materials and Atoms, **269**:3180, 2011

3. AMS of ^{36}Cl With the VERA 3 MV Tandem Accelerator
   M. Martschini, P. Andersson, O. Forstner, R. Golser, D. Hanstorp, A. O. Lindahl, W. Kutschera, S. Pavetich, A. Priller, J. Rohlén, P. Steier, M. Suter, and A. Wallner
   Nuclear Instruments and Methods in Physics Research Section B: Beam Interactions with Materials and Atoms, **294**:115, 2013

4. Light Induced Suppression of Sulfur in a Cesium Sputter Ion Source
   M. Martschini, J. Rohlén, P. Andersson, R. Golser, D. Hanstorp, A. O. Lindahl, A. Priller, P. Steier, and O. Forstner
   International Journal of Mass Spectrometry, **315**:55, 2012

5. Resonant Photoemission at the Iron M-edge of $Fe(CO)_5$
   E. Sistrunk, J. Grilj, B. K. McFarland, J. Rohlén, A. Aguilar, and M. Gühr
   The Journal of Chemical Physics, **139**:164318, 2013

6. Feasibility of Photodetachment Isobar Suppression of WF with Respect to HfF
   T. Leopold, J. Rohlén, P. Andersson, C. Diehl, M. Eklund, O. Forstner, D. Hanstorp, H. Hultgren, P. Klason, A. O. Lindahl, and K. Wendt
   International Journal of Mass Spectrometry, **359**:12, 2014

Declaration

I have during my time as a Ph.D. student taken part in research leading to 12 publications. Of these, I have selected six papers that focus on fundamental questions to be included in my Ph.D. thesis. The six papers listed as additional papers were not included in the thesis in order for it to have a central theme. Papers 2, 4 and 6 have been summarized in my Licentiate thesis *Negative Ions in Accelerator Mass Spectrometry* (2012). In that thesis, the concepts of accelerator mass spectrometry is discussed and the work contained in the three papers are put into its context. Paper 3 is also related to mass spectrometry. Papers 1 and 5, finally, are outside the field of negative ions.

My contribution to the appended papers are as follows:

- Paper **I** and **III**: I participated in the planning, experimental work and analysis of the experiment with AOL. AOL wrote the manuscript and I contributed to its finalization.

- Paper **II**: I participated in the planning, experimental work and analysis of the experiment with AOL. AOL wrote the first draft of the manuscript. I was responsible for the final version of the manuscript as well as the submission process to the journal.

- Paper **IV**: I was main responsible for the planning, experimental work and analysis of the experiment. I wrote the first draft of the manuscript and handled the submission process.

- Paper **V**: I played a major part in the discussion that lead up to the design of the new field ionizer setup. TL performed the simulations and the assembly of the ionizer. I was responsible for the planning, experimental work and analysis of the experiment. I wrote the first draft of the manuscript.

- Paper **VI**: I participated in the experiments and assisted in the final stages of the manuscript preparation.

1

Introduction

The development of quantum mechanics in the beginning of the 20th century was certainly one of the most important scientific breakthroughs in the last century. It has helped scientists in a broad range of fields to understand macroscopic phenomena on a microscopic level. Without it, much of the technology that surrounds us would not exist today. A few examples are lasers, light emitting diodes, computers, nuclear power and GPS navigation.

Quantum mechanics was first and foremost developed in order to understand the observed properties of atomic systems. Bohr, for example, developed his theory in 1913 in order to explain the discrete electron transitions observed in hydrogen. Even though it is still used as an example in high school physics, the Bohr model fails to predict anything more advanced than hydrogen-like systems. A more complete framework is contained in the Schrödinger and Dirac equations for non-relativistic and relativistic systems. In principle, many quantum-mechanical system can be understood by defining a correct non-relativistic Hamiltonian for the system and solving the Schrödinger equation. However, for all but the simplest systems an analytical solution cannot be found. Thus, a large part of forming quantum mechanical models involve applying approximations without removing information relevant to the system of interest. Even so, most systems cannot be solved analytically. Instead, numerical methods have to be used to find the solutions. As a result, experimental observations of atomic systems are of great importance since they serve as benchmarks for the assumptions made in atomic theory. By exploring many different systems and conditions, scientists

have been able to gain a deep understanding of the quantum mechanical world of atoms.

Negative ions are the subset of quantum systems that have a net negative electric charge. They are formed by neutral atoms or molecules capturing one or more electrons. In a typical atomic system, each electron experiences a Coulomb attraction to the positively charged nucleus and a Coulomb repulsion from the other electrons in the system. A common approximation in theories for atoms is to assume that each individual electron only moves through the repulsive mean field created by the other bound electrons. Thus, the total energy of the system is not dependent on the position of each individual electron. This approximation is called the independent particle model and it can be applied successfully to many atomic systems. On the other hand, valence electrons in negative ions experience less Coulomb attraction than those in neutral atoms. Thus, the Coulomb repulsion between the valence electrons will be of higher importance in negative ions than in neutral atoms. Therefore, significant electron correlation is required to bind all the electrons needed to form a stable negative ion. This can easiest be visualized with the prototype negative ion H^-, consisting of one proton surrounded by two electrons. Here, it is obvious that the lowest energy state of the system is when the electrons are located on opposite sides of the nucleus. Clearly, the electrons are highly correlated. Therefore, the independent particle model cannot be used for negative ions since it does not include any correlation effects. Negative ions thus present perfect test systems for the more advanced assumptions that are used in atomic theory of highly correlated systems.

Negative ions was first observed in gas-discharges in the early 20th century by J. J. Thompson [1]. Even so, research on negative ions did not attract much attention experimentally until Wildt, in 1939, proposed that photodetachment of H^- might be responsible for the opacity of the sun's atmosphere [2]. This prediction motivated Branscomb *et al.* to measure cross sections for H^- photodetachment [3]. Their results finally proved Wildts predictions to be correct. While Branscomb pioneered experimental studies on negative ions [4–6], Massey did the same for theoretical calculations. In the book "Negative Ions", first published in 1938, Massey gives a comprehensive review of the theoretical framework of negative ions. The third edition was published in 1976 and is still a relevant source of information [7]. Two modern reviews of both experimental and theoretical nature were published separately by T. Andersen [8] and D. J. Pegg in

2004 [9]. Today, the binding energies of negative ions of most elements in the periodic table have been measured [10]. In addition, many molecular negative ions and clusters have been studied [11].

Doubly excited states, i.e. quasi-bound states that involve the simultaneous excitation of two electrons, are quantum systems where electron correlation is extremely important [12]. Therefore, they serve as an even finer probe for atomic theory than ground states of negative ions. Doubly excited states are most easily investigated in two-electron systems. He and H^- are the only pure two-electron systems available for neutral atoms and negative ions. Doubly excited states in He was first studied by Madden and Codling [13] in the 1960s. Domke *et al.* [14] later improved the resolution of the experiments significantly. H^- was not investigated in detail until 1990 when the group of Bryant [15, 16] published experimental data and Sadeghpour and Greene [17] published a theoretical study.

Experiments on both He and H^- require large excitation energies that can only be supplied by synchrotrons and relativistic beam facilities. An alternative approach that require less excitation energy is to investigate doubly excited states in the alkaline earths for neutral atoms and the alkali metals for negative ions. Since these systems consists of two valence electron outside closed shells, they can be considered to be effective two-electron systems. The alkaline earths have been studied using multi-photon laser excitations [18]. Doubly excited states in the alkali negative ions present favourable experimental conditions since their small binding energies allow experimental invesitagions using standard lasers. Therefore, doubly excited states in the negative ions of the alkali metals have recently been studied in great detail [19–23].

Negative ions are not only investigated to increase our understanding of atomic systems. They are also commonly found to be important in many areas of the natural sciences. For chemists working with solutions, the notion of negatively charged atoms and molecules is nothing new. Here, the polar molecules of the solution can stabilize the otherwise fragile negative ions and they are thus involved in almost all chemical reactions. Furthermore, positive ions have been shown to be abundant in the interstellar media [24]. Since charge is conserved, the missing negative charge either exists as free electrons or negative ions. Therefore, negative ions have long been proposed to exist in the interstellar media [25]. Both positive and negative ions are now considered to be important for the formation of large molecules in space. Interestingly, it is just

recently that negative ions was first detected in the interstellar media [26] and the interest in both laboratory and observatory studies of suitable negative ions are gaining interest [27, 28].

The creation and manipulation of negative ion beams have been used in several applications. One such application is accelerator mass spectrometry which is an analytical technique used for radiological dating. Carbon-14 dating is the first and perhaps the most famous application of this method [29, 30]. A technique based on positive ion beams would have problems due to contamination of nitrogen-14. Fortunately, nitrogen does not form atomic negative ions. Thus, by using negative ion beams in the first stage of the measurement apparatus, all background sources due to nitrogen are removed. Today, many more radio-isotopes are used for dating of a broad range of processes [31]. Another application of negative ion beams is the planned final heating mechanism in the ITER fusion reactor [32]. The magnetically confined plasma cannot be heated to the temperatures needed by electromagnetic fields alone. A neutralized 40 ampere(!) beam of H^- will be used in order to reach the temperatures needed for fusion through collisions between the neutralized H^- and the particles in the plasma.

This thesis is focused on experimental studies of negative ions in an effort to increase our understanding of highly correlated systems. Papers **I** and **II** focus on studies of doubly excited states while Papers **III** and **IV** investigate the break up process itself. All these phenomena have been investigated using an apparatus capable of final state selective measurements of partial cross sections. Careful analysis of these cross sections have resulted in new insights into negative ion physics as well as in general atomic physics. Paper **V** describes the design of a new experimental apparatus which should enable future studies of these phenomena all the way up to the double electron detachment limit. Finally, paper **VI** describes investigations of a rare combination of bound states in negative ions of lanthanum that can lead to the first laser cooling of a negative ion.

2

Negative Ions

In atoms, the positive charge of the nucleus is balanced by the negative charge of the bound electrons, creating an electrically neutral system. Electrons residing in filled shells screen some of the nuclear charge from the outer valence electrons. Nevertheless, the valence electrons are strongly bound by Coulomb attraction to the net positive charge of the combined nucleus and core electrons. In order to form a negative ion, an extra electron has to bind to the neutral atom. As the extra electron is approaching the atom, there is no first-order Coulomb attraction between this electron and the atom. Instead, higher order Coulomb interactions are responsible for the binding. Firstly, the Coulomb action of the extra electron on the atomic valence electrons polarizes the atom, creating an induced dipole. This effect in turn creates an attraction between the extra electron and the dipole which provides a binding force. Secondly, when the extra electron penetrates the charge cloud of the other electrons in the atom the screening of the nucleus will be reduced. Therefore, the attraction between the nucleus and the extra electron will increase. Even tough these two effects are weaker when compared to the direct Coulomb interaction, they still allow the binding of an extra electron for almost all elements in the periodic table [10].

2.1 Basic Properties of Negative Ions

The binding energy of a negative ion is referred to as the Electron Affinity (EA) of the corresponding neutral atom. Negative ions usually have binding energies that are an order of magnitude smaller than neutral atomic systems. For example, the EA of carbon is 1.26 eV [10] while its ionization potential is 11.26 eV [33]. This reduction in binding energy is due to the lack of long range interactions that reduces the depth of the potentials experienced by the extra electron in a negative ion.

In neutral atoms and positive ions, there exists an infinite number of bound excited states due to the long range Coulomb interaction. In negative ions, on the other hand, the short range interactions cannot support an infinite series of excited states. In general, only the fine and hyperfine splittings of the negative ion ground state term are bound. In phosphorus [34] for example, there exists three bound fine structure components of the ground state. In some cases, e.g. C^- [35], more than one term of the ground state can be bound. Almost no negative ions have excited bound state of opposite parity with respect to the ground state. Thus, no dipole optical transitions are generally allowed between any bound states of a negative ion. The only known exceptions are a few elements of the lanthanide series. These many-electron systems exhibit electron correlation strong enough to bind many excited states, some which have opposite parity with respect to the ground state. Prior to this work, the elements known to have bound states of opposite parity are the negative ions of osmium [36–38] and cerium [39, 40]. Apart from these, theoretical studies indicate that several more negative ions of lanthanides should have excited states with opposite parity with respect to the ground state [41]. In Paper **VI** we show that this indeed is the case for the negative ion of lanthanum. In this negative ion, we observed a large number of bound states of opposite parity with respect to the ground state.

2.2 Photodetachment Thresholds

From the discussion in the previous section it is clear that the lack of bound states with opposite parity hinders the investigation of negative ions utilizing optical dipole transitions. The only possible optical process left is photodetachment. In the photodetachment process an electron is ejected from a negative ion following

the absorption of a photon. This process is equivalent to photo-ionization, but since the residual system is neutral, the term ionization is not used. From energy conservation it is obvious that the photodetachment process only can occur if the photon has more energy than the EA of the negative ion. Fortunately, for most photodetachment experiments the small binding energies involved permits the use of light which easily can be produced with commercially available lasers.

Photodetachment can occur from any combination of an initial states in the negative ion to a final state in the residual neutral atom. For example, Paper **II** describes a measurement of the photodetachment cross section of Cs^- when the residual Cs atom is left in the $10\,^2S$ state. Obviously, a larger excitation energy than the EA of Cs needs to be supplied in order to induce this process. However, the principles for the process are the same as in the previously discussed ground to ground state process. Each possible final state combination is usually called a photodetachment cross section channel. In this thesis, a photodetachment channel originating from the negative ion ground state is referred to by the element name followed by the final state in the residual atom in parenthesis, e.g. $Cs(10\,^2S)$.

In photodetachment, the electron is moving far away from the neutral atom. Thus, the penetration effect discussed previously does not significantly contribute in the process. The interactions felt by the outgoing electron can thus be approximated by the centrifugal and polarization term. The resulting effective potential (in atomic units) is

$$V(r) = \frac{\ell(\ell+1)}{2\,r^2} - \frac{\alpha}{2\,r^4}. \tag{2.1}$$

Here, r is the radial coordinate, ℓ is the angular momentum of the outgoing electron and α is the dipole polarizability of the residual atom. In 1948, Wigner [42] realized that for large r, i.e. at small energies above threshold, the centrifugal term dominates the effective potential . Using this assumption, he derived an analytical expression for the shape of the cross section near threshold energy:

$$\sigma \propto (E_\gamma - E_{th})^{(\ell+1/2)}, \tag{2.2}$$

where E_γ represents the photon energy, E_{th} is the threshold energy (usually, but not always, the EA), and ℓ is again the angular momentum of the outgoing electron. Interestingly, by comparing this so called Wigner law to experimental data, one can both infer the EA of the negative ion and the angular momentum

of the initial state. It is an excellent example where the asymptotic behavior of a complex system can yield surprisingly simple results. The Wigner law has been experimentally tested in many experiments and is found to agree extremely well with measured photodetachment cross sections close to the threshold energy [34, 43].

The Wigner law is only valid close to the threshold energy. As the excitation energy is increased, the assumption used in the derivation of the law starts to break down. Usually, the range of validity of the Wigner law is assumed to be the point where the observed cross section deviates from the measured cross section by a fixed amount, typically 5–10%. Several efforts have been made to extend the range of validity for the Wigner law [44, 45]. Papers **III** and **IV** describe investigations of photodetachment to partial cross section channels with extreme values of the final state polarizability. Here, the Wigner law breaks down completely and a new threshold behavior is observed.

2.3 Doubly Excited States

Even tough negative ions usually only have a few bound excited states, a large spectrum of short lived doubly excited states can be found in the photodetachment continuum. They are called doubly excited states because they involve the simultaneous excitations of two electrons. These states are analogous to the auto-ionizing states found in neutral atoms and positive ions. The amount of electron correlation needed to form these states is much larger than what is needed for the ground state of the negative ion. It is thus another important test case for atomic theory involving electron correlation.

Doubly excited states are observed as modulations in photodetachment cross sections. These so called resonances are quantum interference phenomena where a process can take more than one path from the same initial to final state. For photodetachment, the initial state is the negative ion while the final state is a free electron and a neutral atom in one of its bound states. Here, the process can follow two distinct paths: either one electron is emitted and one is excited instantly or two electrons are excited into a doubly excited state that then decay. These processes are illustrated in Fig. 2.1. A doubly excited state can be characterized by its energy, E_r, and width, Γ. The energy is a measure of the excitation energy needed to form the doubly excited state and the width is

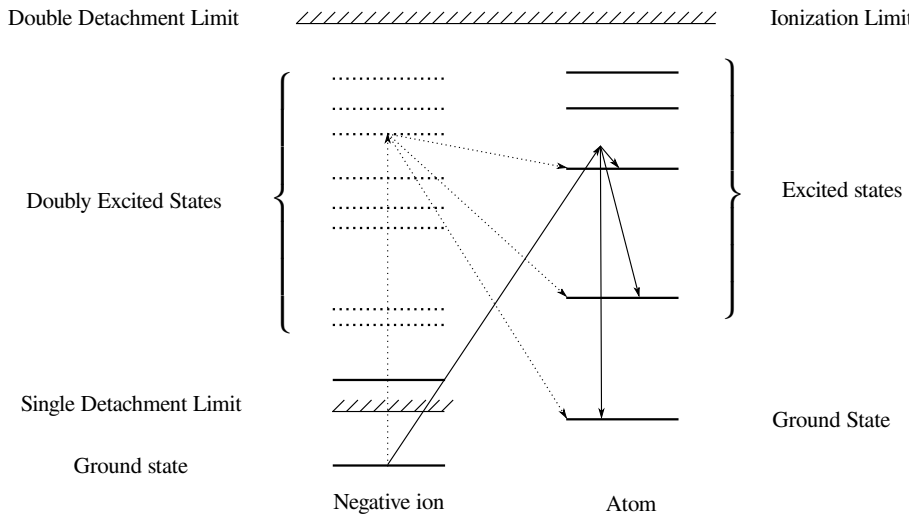

Figure 2.1: Schematic overview of a typical energy level scheme pertinent to studies of doubly excited states. Solid and dotted horizontal lines represent bound and quasi-bound states, respectively. Solid arrows represent the direct photodetachment path, ejecting one electron and exiting the other. Dotted lines represents the resonant path via a doubly excited state. The existence of two paths from the same initial to final state creates modulations in the observed cross section.

determined by its life time. Both the energy and width have units of energy. A doubly excited state can in principal cause a resonance in all energetically available photodetachment channels. However, the width and energy are properties of the state and not the resonance. Therefore, the same width and energy should be observed in all channels for each doubly excited state.

Photodetachment is in principle a scattering problem of a neutral atom and a free electron. Thus, much of the frame-work on scattering phenomena can be applied to photodetachment as well. In both areas, two types of resonances are generally observed, called Feshbach and Shape resonances. Feshbach resonances involve doubly excited states that are bound with respect to a state in the neutral atom that is not energetically accessible. Shape resonances, on the other hand,

involve doubly excited states that are bound just above its parent state.

The shape of the modulation of the non-resonant cross section for a resonance caused by a doubly excited state can be described by a Fano profile[46]. Shore later derived an equivalent parametrization,

$$\sigma_{\mathrm{mod}} = \frac{a\epsilon + b}{\epsilon^2 + 1}, \tag{2.3}$$

that is more commonly used [47]. Here, a and b are the so called Shore parameters and $\epsilon = (E_\gamma - E_r)/(\Gamma/2)$ is a dimensionless energy parameter. By multiplying the Shore expression with a non-resonant background cross section one obtains the total cross section. The width and energy of observed resonances can be extracted by applying numerical fits. It should be noted that the resonance profiles of Shore and Fano only are valid for single isolated resonances. An alternative parametrization treating overlapping resonances are described in paper **II**.

Doubly excited states are per definition two electron systems. Thus, it is beneficial to study them in atomic two-electron systems in order to reduce the complexity of the observed cross sections. H^- is the only true two electron negative ion and it has thus been studied extensively [16, 23, 48–50]. Unfortunately, these systems requires large excitation energies that can only be achievable at larger experimental facilities (synchrotrons or relativistic ion beams). Instead, atoms and ions with two electrons outside filled shells, so called quasi-two electron systems can be investigated. Negative ions of the alkali metals have turned out to be good experimental systems for studies of doubly excited states [19–21, 51–54]. Papers **I** and **II** present investigations of doubly excited states of negative ions of potassium and cesium, respectively.

3

Resonant Ionization Spectroscopy

All experimental work presented in this thesis is based on Resonance Ionization Spectroscopy (RIS). A short introduction to the history and concept of the method is therefore given in this section.

RIS is a light-based technique that was developed in the mid 70s as a means to efficiently and selectively measure properties of neutral atoms. The method was first developed by Hurst *et al.* in order to measure the lifetime of the $2\,^1\mathrm{S}$ state in Helium [55].

In its simplest form, RIS is a two step process involving two photons with the same energy. Firstly, a photon resonantly excites an atom from a lower to an upper state. Secondly, the now excited atom is ionized by a second photon from the same light source. Most absorption lines in atoms are element specific, and this method hence gives a very high elemental selectivity. The key aspect for the success of RIS is the fact that the process only occurs if the photons have an energy that matches an absorption line in the atom. This fact can be utilized for analytical as well as spectroscopic investigations.

A limitation of the simple RIS-scheme is the efficiency of the ionizing step. In this basic scheme, the ionization is caused by photo-ionization which unfortunately is a non-resonant process with a very small cross section. Therefore, it is usually required to use high power lasers in order to achieve adequate signal

levels. This laser power requirement can pose a problem for atomic spectroscopy where narrow bandwidth continuous-wave lasers are needed in order to perform high-precision measurements. The power of the laser can be increased by using pulsed lasers, but this is only an option in experiments where the requirement of the energy resolution is lower. Furthermore, using pulsed lasers reduces the duty cycle in the experiment. This might be problematic in cases where the production of the atoms or ions under study is low.

If photo-ionization has to be used, there are two tricks that can be employed in order to increase the efficiency of the process. Firstly, the cross section for photo-ionization is at its maximum just above threshold and gradually decreases as the excitation energy is increased. Therefore, the ionizing laser should always be tuned to just above the ionization potential. Secondly, if there are known auto-ionizing resonances available for the system, the efficiency can be increased by several orders of magnitude by tuning the laser into resonance with one of the auto-ionizing states [56].

If photo-ionization is not a requirement for the implementation of the RIS scheme, the ionization efficiency can be increased significantly by using other ionization processes. By using e.g. collisional ionization or electric field ionization, discussed in the next section, only the resonant steps in the scheme need to be saturated. These processes completely eliminates the need for high power lasers for the ionizing step [57].

Modern RIS-schemes use several tunable lasers in order to further increase the selectivity and efficiency of the method. I will here describe in some detail one such example. Recently, Roethe *et al.* [58] used RIS to measure the ionization potential of astatine at the radioactive beams facility ISOLDE at CERN [59, 60]. Astatine is highly radioactive with the most long lived isotope having a half-life of 8.1 hours. This short half-life makes it extremely hard to study in the lab. Therefore, Roethe *et al.* used a RIS scheme involving several tunable lasers to resonantly ionize astatine atoms inside an ion source. Astatine was produced by bombarding an uranium-carbide target with a high energy proton beam. Production of astatine was measured by detecting its radioactive decay when implanted in a metal foil. The ionization potential of astatine was determined by scanning one of the resonant steps over a series of Rydberg states close to the ionization threshold. By extrapolation, the ionization potential was determined with high precision.

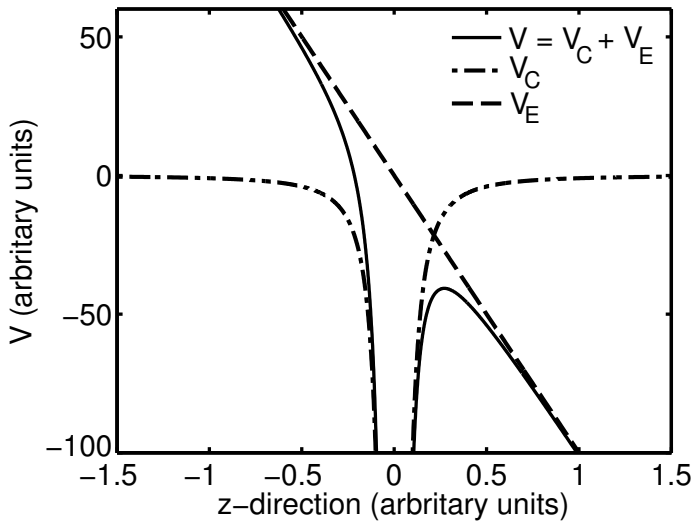

Figure 3.1: Potential for an electron bound in a coulomb field influenced by an external electric field.

3.1 Field Ionization

The experimental apparatus used in all the papers presented in this thesis utilized field ionization as the final ionizing step in the RIS scheme. Field ionization is the process whereby an electric field, if strong enough, can ionize loosely bound atomic systems.

The field ionization mechanism is schematically shown in Fig. 3.1. A linear electric potential $V_E = zE\hat{z}$ is applied to an electron bound in a coulomb potential $V_C \propto 1/r^2$. Unperturbed, the coulomb potential can bind an infinite number of states. As the applied external field increases the potential is bent and any states that lie above the barrier of the effective potential will be ionized. With increasing electric field strengths, more and more states will be ionized. Ionization of bound states can occur due to tunneling through the barrier. However, tunneling is negligible in most practical cases.

The electric field strength needed for field ionization is given by the empirical formula [57, 61]

$$E \approx 3 \times 10^8/(n^*)^4 \text{ V/cm}, \tag{3.1}$$

where n^* is the effective quantum number of the field ionized Rydberg atom. Both the pre-factor and the exponent on n^* have been seen to vary slightly between experimental setups, but Eq. (3.1) gives a good indication of the fields necessary for field ionization. From Eq. (3.1) it is clear that only relatively loosely bound atoms can be field ionized as the required field strength grows rapidly with decreasing n^*.

3.2 RIS Scheme Used in the Papers

The same type of RIS-scheme is used in all the experiments described in Papers **I**–**V**. The scheme of paper **IV** is described below as an example. The experiment described in Paper **VI** also used the RIS method. However, in that experiment the simple RIS-scheme described in the beginning of this chapter was used. Full details can be found in the experimental section of the corresponding paper.

In paper **IV** the three step RIS scheme shown in Fig. 3.2 was used in order to measure the photodetachment cross section of the process

$$\mathrm{Na}^- + E_\gamma \rightarrow \mathrm{Na}(5\,^2G) + e^-.$$

In the experiment, a 6 keV beam of Na^- ions is exposed to a single UV laser pulse, marked by γ_{UV} in Fig. 3.2. This laser pulse initiates the photodetachment process and all energetically available states in Na will be populated in this step. The cross section of the process can be measured by scanning the photon energy of this first step. The photodetachment process is much faster (∼fs–ps) than the pulse length of the laser (∼ns). Therefore, the ions in the ion beam can be considered to be stationary for the duration of the laser pulse. Most atomic states involved have lifetimes on the order of 10 ns – 1 µs. Thus, as soon as possible after the UV pulse an IR laser pulse, marked by γ_{IR} in Fig. 3.2, resonantly excites Na atoms in the $5\,^2$G state to the $23\,^2$F Rydberg state. In practice, the width and jitter of the laser pulses sets a limit of the temporal separations between the two pulses. The delay can be set to approximately 20 ns without pulse overlap. This short delay permits only a small fraction of the excited atoms to decay before they are exposed by the second laser pulse. The absorption line used in Na is unique and no other populated states will be resonantly excited by the IR pulse. Therefore, they will not contribute to the signal. After the second laser pulse, the atoms in the $23\,^2$F state travel downstream to a field ionizer.

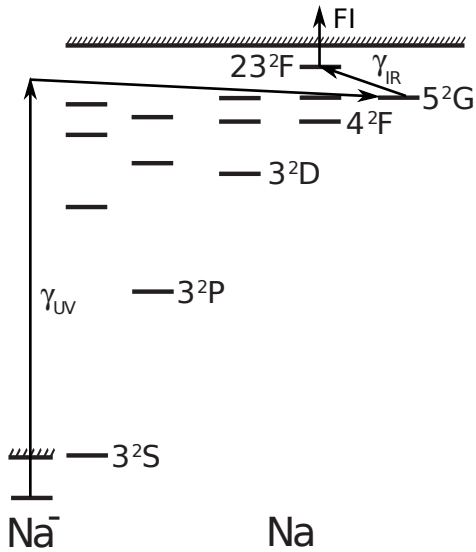

Figure 3.2: Schematic overview of the RIS scheme used in paper **IV**.

The time of flight is usually a few μs. Highly excited Rydberg states have life times on the order of 10 μs [62]. Therefore, only a small fraction of the Rydberg atoms will decay before being detected. In the field ionizer, the final, ionizing, step in the RIS scheme is performed.

The field ionizing step is not only used to increase the ionization efficiency of the scheme, but also to improve signal to noise conditions in the experiment. Since negative ions are loosely bound, they have a large collisional cross section compared to positive ions. This leads to a substantial background of positive ions that are created by collisions with rest gas in the interaction region. In addition, sequential absorption of two UV-photons also produces positive ions. These positive ions will interfere with the small signal of positive ions from the RIS-scheme. Therefore, the signal and background is separated by using the properties of field ionization. The field ionizer can be designed to field ionize the Rydberg atoms at a non-zero electric potential. Consequently, they will acquire a different kinetic energy than positive ions from background processes which are created at ground potential in the interaction region. A kinetic energy analyzing element can therefore be used to create a spatial separation of the signal and background sources created in the experiment. Finally, a position

sensitive detector is used to measure ion events stemming from the field ionized ions only.

4

Experimental Apparatus

A highly specialized experimental apparatus is needed to investigate the phenomena described in chapter 2. The work presented in Papers **I-V** was performed at the *Gothenburg University Negative Ion Laser LAboratory* (GUNILLA), while the experiment presented in Paper **VI** was performed at the Department of Physics at Denison University. A detailed description of the experimental apparatus used at GUNILLA and Denison University can be found in Refs. [63] and [40], respectively. The two setups are similar and large parts of the description of GUNILLA also applies to the apparatus at Denison University. The main difference between the two facilities is that it is only possible to perform crossed beams measurements at Denison University.

GUNILLA consists of an ion beam apparatus that both produces and transports a beam of negative ions of interest to one of two interaction regions. In the selected interaction region, the ion beam is overlapped with one or more laser beams and the resulting photodetachment products are detected and analyzed. All experiments are performed in vacuum. In the interaction regions, the pressures are typically a few 10^{-9} mbar. A schematic overview of the complete setup can be seen in Fig. 4.1.

The two interaction regions can be used to perform either collinear or crossed beams experiments. The collinear setup has a large sensitivity due to a large interaction volume. Therefore, processes with small cross sections can be efficiently studied using this setup. Unfortunately, the overlap between the laser and ion beams can only be estimated from the geometry of the system. Thus,

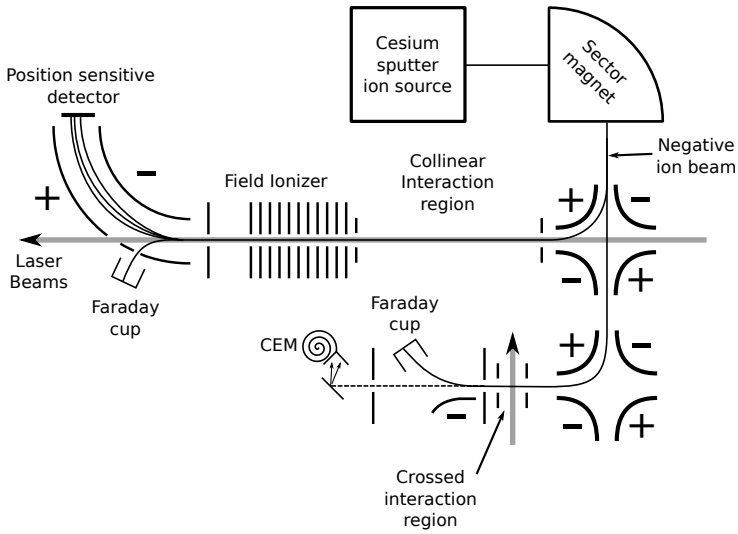

Figure 4.1: Schematic overview of the components that make up GUNILLA.

absolute cross sections cannot be measured with good precision. Consequently, most experiments performed with the collinear setup is only used to measure relative cross sections.

If precise absolute cross section measurements is of interest, the crossed beams setup can be used instead. Here, the laser beam is scanned through the ion beam using the animated beams method developed by Defrance *et al.* [64]. Using this method, the overlap is indirectly measured and precise absolute cross section measurements can be performed. However, due to the reduction in interaction volume the sensitivity of the apparatus is greatly reduced compared to the collinear setup. The crossed beams setup is not used in any of the papers presented in this thesis. Details on the design of the crossed beams setup is therefore referred to the work of Leopold *et al.* [65].

4.1 The Ion Beam Apparatus

At GUNILLA, negative ions are produced by a commercial cesium sputter source based on the design of Middleton [66]. This type of ion source was designed to create intense beams of primarily atomic negative ions for applications in

accelerator mass spectrometry. It is the most efficient negative ion source for almost all negative ions of the periodic system. However, loosely bound or metastable negative ions such as Ca^-, Be^-, B^- and He^- are more efficiently produced from positive ions undergoing charge exchange with alkali or alkaline earth metals [67, 68].

In the cesium sputter source, Cs^+ ions are accelerated to high energy onto a sample that is continuously coated with a layer of neutral Cs. The Cs^+ ions sputters atoms out of the sample material. The low work function of Cs provides the perfect environment for the sputtered atoms to capture an extra electron. The energetic sputtering process produces ions with a large internal energy which makes it especially useful for spectroscopy of excited states in negative ions. Unfortunately, the spread in the initial kinetic energy of the ions is quite large. This energy spread will reduce the resolution of the experiment through Doppler broadening. Therefore, it is necessary to accelerate the negative ions to keV kinetic energies in order to compress the energy spread [69].

Ions created in the source are extracted and accelerated to a final kinetic energy of 6 keV. Several ion optical elements guide and shape the ion beam on the path to the interaction region [63]. All elements are electrostatic except for a 90° sector magnet. Finally, the ion beam reaches the interaction region consisting of two 3 mm diameter apertures placed 610 mm apart. A grounded steel tube encloses the interaction region in order to shield it from stray electric fields.

The 90° sector magnet is used as a mass dispersive element in order to isolate only one mass to charge ratio. The whole system has a mass resolution of approximately 500 u and 800 u for atomic and molecular species, respectively. The discrepancy in the mass resolution actually gives insight into some interesting physics. The mass resolution depends on the energy spread of the ions. The larger mass resolution for molecular ions indicate that they are created with a more narrow energy distribution when compared to atomic ions. This difference can be attributed to the process by which the ions are created. For atomic ions, a more direct process is assumed whereby a Cs^+ ion transfers some of its energy directly to an atom resulting in a rather large spread of initial kinetic energies. Molecules, on the other hand are most likely created at the surface of the sample through more complex reactions and are thus formed at thermal energies. Experimentally, this can be observed in recorded mass spectra where atomic

negative ions are seen to have a tail towards higher masses while molecules have symmetric mass peaks.

An important parameter that defines the ion beam system is its transmission, i.e. the fraction of the ions produced in the ion source that reach the end of the interaction region. According to Liouville's theorem, the area of the phase-space of an ion beam is conserved. If the divergence of the ion beam is reduced, the geometrical size has to increase. A sputter ion source creates a strongly diverging ion beam. Since the collinear interaction region only transmit a 3 mm wide and parallel ion beam, the transmission of the apparatus is expected to be low. Theoretically, the transmittance is limited by the emittance of the ion source and the acceptance of the interaction region which are 50π mm mrad and 3.7π mm mrad, respectively. This results in a theoretical upper bound of 0.5% transmission for the complete apparatus.

4.2 Laser Systems

Photodetachment is a non-resonant process with a very small cross section. Therefore, high power lasers are needed in order to increase the probability to induce the process. Nano second pulsed lasers provide the photon flux needed while retaining a bandwidth useful for spectroscopic investigations. The duty cycle is also reduced, which for these experiments actually are beneficial. By using time-gating of the data collection, collisional detachment with rest gas in the vacuum chamber can be reduced significantly.

There are two pulsed tunable laser systems available at GUNILLA. Both lasers consists of Optic Parametric Oscillators/Amplifiers (OPO/OPA) systems pumped by Nd:YAG lasers. One covers the wavelength range 220–1800 nm and the other covers 1350–5000 nm. The performance of each laser is similar: they both have a repetition rate of 10 Hz, a pulse length of approximately 5 ns, a bandwidth of 0.2 cm^{-1} and a pulse energy of 1 mJ. The lasers can be controlled externally and synchronized to each other with an accuracy of approximately 10 ns. The laser producing light in the 220-1850 nm range is pumped by the third harmonic of the Nd:YAG laser. The laser producing light in the 1380-5000 nm range is pumped by the fundamental of the Nd:YAG laser. However, the laser is seeded by an oscillator pumped by the second harmonic of the Nd:YAG laser. The combination of near infrared OPO seeding of a mid infrared OPA gives

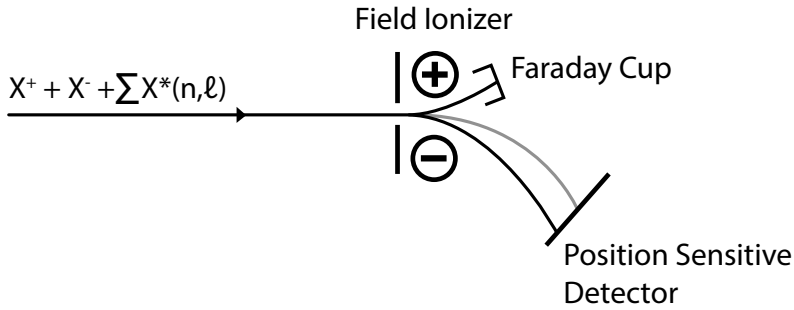

Figure 4.2: Schematic overview of the detection system used in the experiments described in Papers **I-IV**.

the laser its unique properties of a narrow bandwidth and a tunable wavelength extending far into the infrared.

4.3 Detection System

The experiments presented in Papers **I-V** all utilize a RIS scheme of the type discussed in Sec. 3.2. In order to efficiently measure a photodetachment channel of interest, a specialized detection system is needed. The measurements in Papers **I-IV** were performed with a setup that is described in great detail in Paper **I**. Paper **V** describes the design and first results of a new detector setup that was developed in order to remedy some of the drawbacks of the old design.

An overview of the detection system used for the experiments presented in Papers **I-IV** can be seen in Fig. 4.2. Both this and the new version consists of three parts: a field ionizer, an energy analyzer, a Faraday cup, and a position sensitive detector (PSD). The field ionizer is used to ionize and velocity tag highly excited Rydberg atoms. The energy analyzer will then create a spatial separation of the field ionized ions as compared to ions created by background processes in the region before the field ionizer. The analyzer is simultaneously used to deflect the residual negative ion beam into a Faraday cup. Finally, the PSD is used to detect the positive ions. The position information can later be used to extract the signal stemming from field ionized ions.

In papers **I-IV**, a combined field ionizer and energy analyzer consisting of

two electrostatic bending rods was used. The rods created an electric field that increased along the central axis. Depending on their binding energy, Rydberg atoms were field ionized at different positions in the field. The subsequent deflection by the same field induced a spatial separation between positive ions from background sources and the Rydberg atoms of interest that could be detected by the PSD. This setup had several drawbacks which reduced the functionality of the detection system. Firstly, the PSD had to be placed close to the ion beam. This introduced both ion and laser induced noise on the detector. Some of this noise could be removed with the help of a pulsed detection scheme. However, for light ions, especially Li^-, this method was not applicable since the time between the laser pulse and the arrival of the positive ions was very short. Secondly, there was no control over the field ionization conditions and the energy separation. This did not limit the experiments presented in papers **I-IV** but for future experiments, it would have been an issue.

The old and new setup differs in the design of the field ionizer and the energy analyzer. The main design goal was to develop a field ionizer that did not affect the direction of the ion and atom beam. In the literature, a common approach to this problem is to use a coaxial electric potential created either by coaxial plates or a resistive tube [70]. This setup yields a linearly decreasing electric potential inside the device that is abruptly terminated by a large step in the electric potential. This potential profile results in an electric field profile that is constant in the first part of the field ionizer and then increases rapidly over a short distance. Therefore, the field ionization will either occur in the beginning or end of the device, depending on the principal quantum number of the Rydberg atoms and the total bias over the device. Rydberg atoms ionized at the end of the tube will acquire a shift in their kinetic energies equal to the bias between the entrance and exit of the device.

The new design builds upon the idea discussed above and can be seen in Fig. 4.3. The field ionizer consists of 12 coaxial circular plates of 1 mm thickness with 4 mm apertures in the center. The first 11 plates are placed to form 5 mm gaps between plates while the final 12th plate is placed to form a 15 mm gap. In total, the field ionizer is thus 77 mm long. Plates 2–12 can be individually biased while the first plate is grounded to ensure a field free interaction region. In this way, a high degree of control over the electric potential, and hence the electric field, between each plate-pair can be achieved.

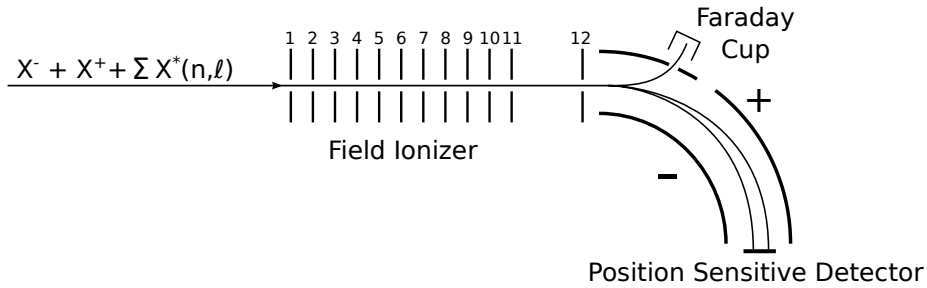

Figure 4.3: Schematic overview of the new detection system used in the experiments described in Paper **V**.

The new field ionizer is not energy dispersive. An energy analyzing element thus had to be inserted in the beam path. The energy analyzer consists of two concentric plates that bends and separates the positive ions. Residual negative ions will be deflected in the opposite direction through a hole in the plate which allows measurements of the current of the negative ion beam.

The new field ionizer setup is designed for three types of experiments: photodetachment cross section measurements with final state selectivity; Rydberg state branching ratios close to the double detachment limit; and an investigation of the threshold law for double detachment. In the next three subsections, SIMION simulations for the three prototype experiments will be presented and discussed. For all simulations, ions and neutral atoms of Cs with a kinetic energy of 6 keV were used. Since the acceptance angle of the collinear interaction region is small, the beam diameter was set to be 3 mm with no divergence.

4.3.1 Photodetachment Cross Section Measurements With Final State Selectivity

Experiments performed in papers **I-V** benefit from a large separation between positive ions created either by background processes or by the signal stemming from field ionized Rydberg atoms selected in the RIS-scheme. A large spatial separation can be achieved by creating a large kinetic energy separation between the background and signal that can be dispersed by the energy analyzer. A suitable potential and field profile for this case can be seen in Fig. 4.4a. Here, the fields have been tuned in order to detect a Rydberg state with $n = 25$, which require a field strength of approximately 750 V/cm in order to be field ionized

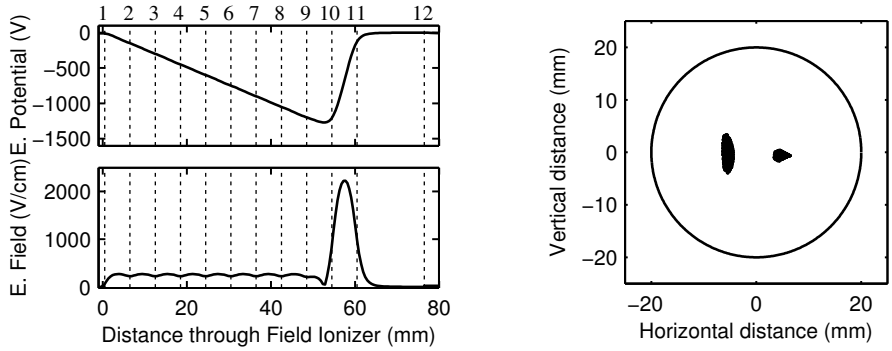

Figure 4.4: Simulated field ionizer scheme for final state selective measurements of photodetachment cross sections. The electric field and potential curves in (a) represents the field along the central axis of the field ionizer. The numbered vertical dashed lines correspond to each plate in the field ionizer. The left and right spots in (b) are positive ions detected by the PSD stemming from background and signal sources, respectively.

(see Eq. (3.1)).

The first ten plates of the field ionizer are biased in order to create a linear decrease in the electric potential. The slope of this potential should be such that the corresponding electric field is smaller than that required for field ionization of the Rydberg state of interest. Finally, the potential is brought back to ground over a single plate-pair. This creates an electric field that is much larger than that required for field ionization. In Fig. 4.4a it is shown that the Rydberg state will be ionized at a potential of approximately -1250 V. Consequently, the field ionized atoms will be decelerated as they fly out of the ionizer, acquiring a final kinetic energy of 4.75 keV. In contrast, ions created outside the field ionizer will maintain their kinetic energy. The field configuration shown in Fig. 4.4a creates an energy difference of 20% between signal and background ions. This is sufficient to separate the two sources of positive ions.

The resulting separation on the PSD is shown in Fig. 4.4b. The left spot is produced by positive ions created outside the field ionizer whereas hits on the right side are positive ions stemming from field ionized Rydberg atoms. The left spot is somewhat elongated horizontally due to the different paths of the two

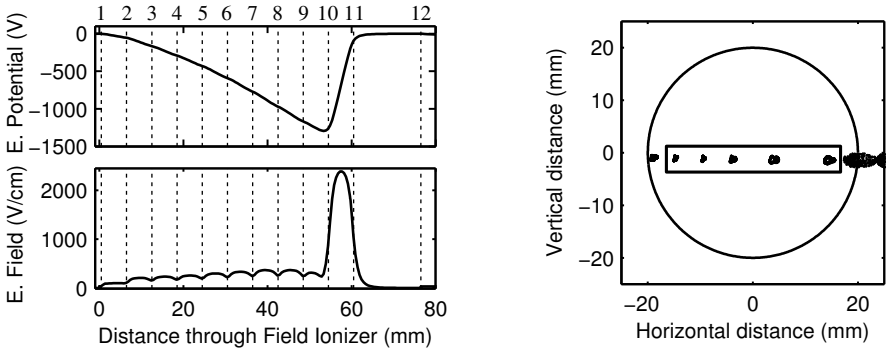

(a) **(b)**

Figure 4.5: Simulated field ionizer scheme for detection of Rydberg state branching close to the double detachment limit. The electric field and potential curves in (a) represents the field along the central axis of the field ionizer. The numbered vertical dashed lines correspond to each plate in the field ionizer. The spots inside the rectangle in (b) shows the positions on the PSD for ions stemming from Rydberg atoms with $n = 31$–35. Hits to the left and right of the region of interest correspond to Rydberg states with $n > 35$ and $n < 31$, respectively.

beams in the energy analyzer. It is obvious that the new field ionization setup is adequate for measurements of partial photodetachment cross sections.

4.3.2 Rydberg State Branching Close to the Double Detachment Limit

Photodetachment with photon energies approaching the double detachment limit represents an interesting aspect of photodetachment. In this case, the residual atom can be left in any of the energetically available Rydberg states close to the ionization limit. With the new detector setup it should be possible to measure branching ratios of a large range of Rydberg states, leading to further insight into the photodetachment process.

An example of a electric potential and field profile tailored for a Rydberg branching measurement is shown in Fig. 4.5a. Here, the goal is to detect Rydberg atoms with $n = 31$–35. The field ionizer is configured to contain three different regions. Plates 1, 2 and 3 are used to field ionize Rydberg states with

$n > 35$ at a potential of approximately -50V. The subsequent plate-pairs 3–4, 4–5, 5–6, 6–7 and 7–8 are tuned to sequentially field ionize each of the five Rydberg states of interest. Each Rydberg state is field ionized at lower and lower potentials. Finally, plates 9 through 11 are used to field ionize Rydberg states with $n < 31$ at a potential of approximately -1250V. This electric potential and field profile will give each of the seven groups of Rydberg states different final kinetic energies. The resulting spatial separation, created by dispersion in the energy analyzer, is shown in Fig. 4.5b. All the seven groups are well separated and the Rydberg states of interest can easily fit on the PSD. Approximately five Rydberg states can be detected at the same time. This limit is set by the size of both the PSD and the ion beam. Field ionizing Rydberg states with n outside the range of interest inside the field ionizer ensures that background contamination of the signal spots on the PSD is minimized.

The range of n-values that can be detected is tuned by shifting the voltages in the field ionizer. The lowest n Rydberg state that can be field ionized by the system is the $n = 13$ Rydberg state. This state requires an electric field of approximately 10 kV/cm. At lower n, a significant distortion of the trajectories of the positive and negative ion beams in the field ionizer is observed. It is more difficult to estimate the maximum n Rydberg state that can be detected. Using Eq. (3.1), one finds that the electric field needed for field ionization between subsequent n Rydberg states differs only a few V/cm at $n = 50$. At such low field differences, it becomes difficult to create a separation in kinetic energy between the Rydberg states. Mainly, offsets in power supplies and stray electric fields will begin to significantly hinder the precision of the applied electric fields in the field ionizer.

4.3.3 Threshold Law for Double Photodetachment

Double photodetachment can occur when the photon carries enough energy to eject two electrons from a negative ion. This is a very interesting phenomena, where two separate theoretical predictions of the shape of the threshold cross section have been presented [71, 72]. There is still no conclusive experiments that prove, or disprove, these theoretical models [73, 74].

For this experiment, the signal from double detachment will be produced as positive ions in the interaction region. Therefore, a RIS-scheme cannot be used to separate the signal from background sources of positive ions that also

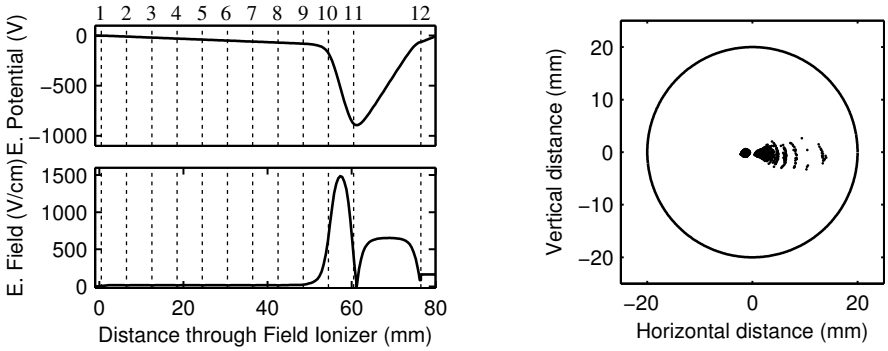

(a) **(b)**

Figure 4.6: Simulated field ionizer scheme for detection of doubly detached negative ions. The electric field and potential curves in (a) represents the field along the central axis of the field ionizer. The left spot in (b) corresponds to positive ions created in the interaction region while hits to the right correspond to field ionized Rydberg states.

are created in the interaction region. The two main background sources of positive ions are collisional ionization with background gas and photo-ionization of residual atoms occupying excited states by the photodetachment laser. The first source can be reduced by lowering the pressure in the interaction region and the second can be reduced by choosing an element with a low ionization cross section. However, there is a third significant background source that can be removed by the field ionizer. In the photodetachment process, highly excited Rydberg states will be populated close to the ionization limit. Such states will be field ionized by the bending plates in the detection setup. If there is no previous energy difference between the Rydberg atoms and positive ions, they will end up on the same position on the detector. This background can be reduced significantly by using the electric field configuration shown in Fig. 4.6a. Here, the lowest permissible increase in the potential bring as many Rydberg states as possible to a lowered potential. A large step in the potential is then introduced to field ionize the Rydberg states. This subsequent deceleration of the Rydberg states results in an energy separation large enough to separate them from positive ions created outside the field ionizer. In Fig. 4.6b, the signal spots on the PSD resulting from Rydberg states and double detachment can be seen to the right and left, respectively. The irregular shape of the signal spot stemming

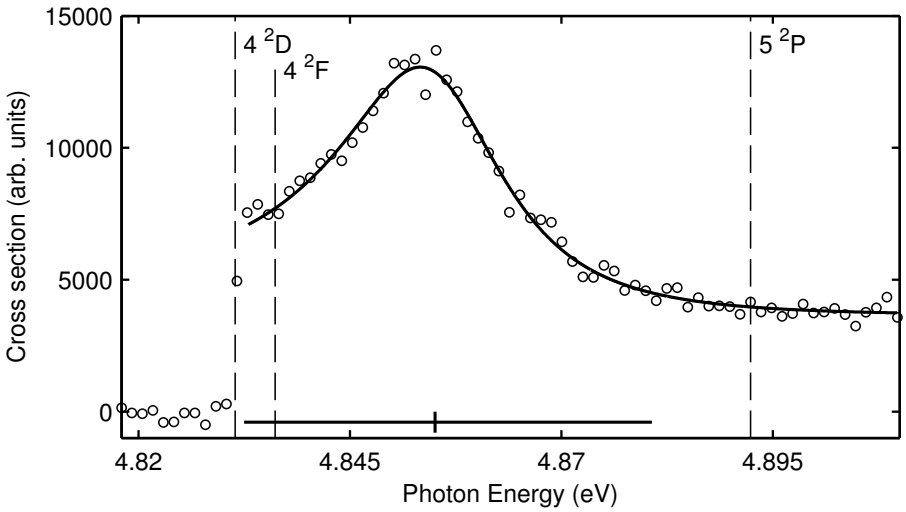

Figure 4.7: Partial photodetachment cross section for the Na($4\,^2$D) channel. The solid line represent a fit to the data of a single shore profile together with a linear background. The vertical and horizontal bar represents the energy and width of the resonance. The dashed vertical lines, finally, indicates the position of channel openings.

from Rydberg states are caused by suboptimal trajectories of the positive ions in the energy analyzer. Simulations show that Rydberg states with n lower than approximately 50 can be separated from the double detachment signal. Further optimization of the apparatus might allow an even lower limit. The experiment on Rydberg branching ratios should result in a good estimate on the amount of contamination that will result from $n > 50$ Rydberg states.

4.4 Data Collection and Analysis

During an experiment, several parameters needs to be measured and stored. Typically, the recorded parameters are: the negative ion current; the laser pulse energy; the photon energy; and position information from the PSD. Since the experiments are pulsed, the timing information of ions arriving at the PSD relative to the laser pulses are also recorded. The time span recorded is usually from a few μs before to a few 10s of μs after the laser pulse. All data is collected

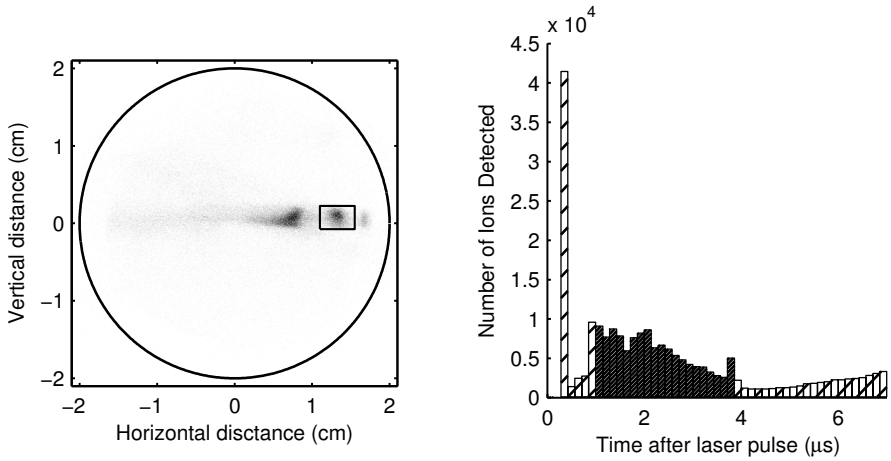

Figure 4.8: Position and time data for the cross section curve presented in Fig. 4.7. (a), typical spatial distribution on the PSD. Darker areas contain more events. The square box indicates the area containing events from the channel of interest. (b), distribution of arrival times of events on the PSD in respect with the laser pulse. The black area contains signal from the channel of interest.

using LabView based software that also controls the scanning of the lasers during the experiments. The collected data has to be processed offline before being analyzed.

The offline analysis is performed in a combination of C# and Matlab programs. The goal is to produce cross section curves like the one shown for the photodetachment channel Na($4\,^2$D) in Fig. 4.7. In the figure, each circle represents accumulated data for approximately 3000 laser shots.

In order to reduce background sources and remove artifacts, only data that fall inside a subset of the parameter space are kept for further analysis. The most important parameter is the time of arrival of ions on the PSD relative to the laser pulse. The transit time of the laser pulses through the interaction region is on the order of ns while the transit time of the photodetached atoms are on the order of μs. This means that the laser pulses effectively define time zero from which it is possible to deduce the expected arrival times at the PSD of ions stemming from atoms created in the interaction region. Thus, by selecting

events that fall into the correct time window, an increase in the signal to noise ratio is achieved. Similarly, by only selecting events found in the expected area on the detector, background sources are reduced further. An example of such cuts is shown in Fig. 4.8. Here, both the cut in position and time reduced the background sources significantly. As can be seen in Fig 4.8a, there is more than one signal spot on the detector. The left part of the signal is due to two-photon absorption of UV-photons and should be excluded. For the timing, seen in Fig. 4.8b there is a large peak due to noise induced by the UV laser pulse. Both background sources would be added to the cross sections curve, but by only selecting data from the regions of interests this background is eliminated completely.

Once the cuts have been applied to the data, the number of hits are normalized to the ion current and number of photons in a laser pulse. Finally the normalized signal is binned according to the photon energy and an average cross section value is calculated for each bin. In order to avoid broken data sets, the excitation energy of the photodetaching laser in the RIS scheme is scanned multiple times over the energy range of interest. Each scan is usually around one hour in length (36000 laser shots). Therefore, the final step in the analysis is to take the average of several normalized scans over the same energy range in order to produce the final cross section curve.

5

Results & Discussion

In this chapter, the results presented in Papers **I-VI** will be summarized. Papers **I-IV** describes experimental studies of photodetachment of K^-, Cs^- and Na^-. These papers cover two main topics: resonances in partial photodetachment cross sections due to interference with doubly excited states and the effect on photodetachment threshold behaviors due to large dipole polarizabilities of the final state channel. The two topics will be covered separately and results from the appropriate papers will be presented under the corresponding section. Paper **V** describes results on Cs^- photodetachment using the new field ionization setup described in Sec. 4.3. Finally, Paper **VI** presents results from a study on bound-bound state transitions in La^-.

5.1 Doubly Excited States

Papers **I** and **II** report on measurements of partial cross sections of photodetachment of K^- and Cs^- to highly excited final state channels.

Previously, Kiyan *et al.* [20] investigated the $K(5\,^2S)$ channel up to an excitation energy of 4.298 eV. A subsequent paper by Liu [22] presented calculations of the same channel as well as several other channels to highly excited states in K. Experimentally, five distinct resonances were found in the cross section data. All were confirmed by Liu's calculations and in addition, two new resonances were predicted to exist at higher excitation energies.

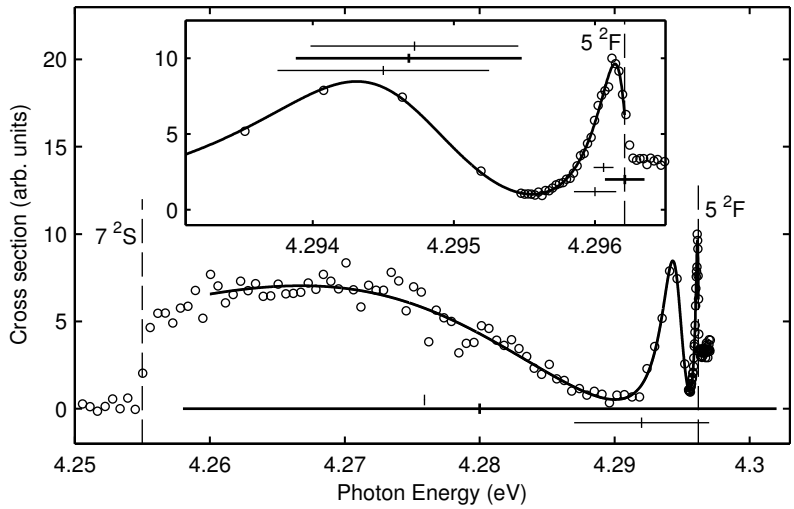

Figure 5.1: Partial photodetachment cross sections in the K($7\,^2$S) channel. Dashed vertical lines indicate channel openings. Open circles represent measured data points and solid lines represent numerical fits as described in the text. The inset figure is a zoom of the larger figure close to the K($5\,^2$F) threshold. The vertical, respectively horizontal, solid lines represents the energy and width of a resonance. Each resonance has three resonance indicators: the one in the middle is from Paper **I**, the one on above is from the theoretical work of Liu [22], and the one below is from the experiment by Kiyan *et al.* [20].

For Cs^-, measurements of photodetachment cross sections have been performed up to 1.96 eV excitation energy [53]. This energy range permits photodetachment that leaves Cs in the ground state or in the first excited state. For a long time, Cs^- was thought to have a bound state close to the photodetachment threshold. However, this $Cs^-(6s6p^3P)$ state was found to be situated in the continuum just above the threshold [75]. Apart from theoretical predictions of the energy of the ^3P state [76, 77] few theoretical publications exist [78].

Paper **I** and **II** have both extended the energy range of investigation compared to previous experiments. In the case of K^- photodetachment, an energy range of 4.25–4.36 eV was covered. This energy region includes, and extends, the range covered by the experiment by Kiyan *et al.*. For Cs^-, the energy range

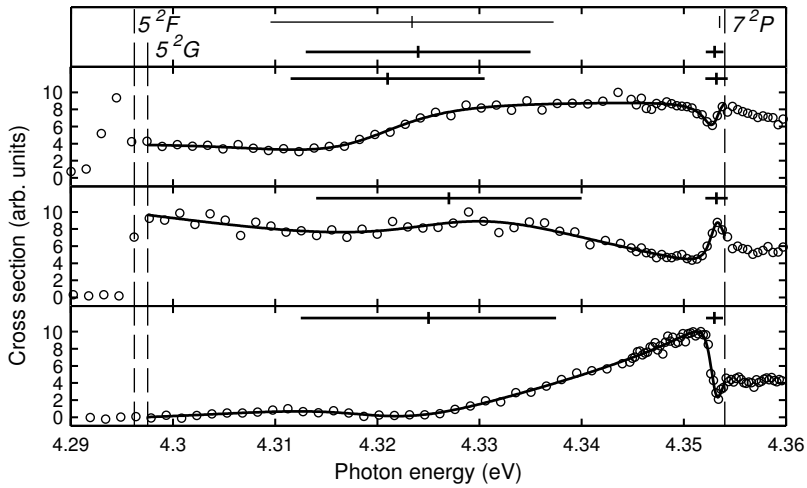

Figure 5.2: Partial photodetachment cross sections in the K(7 ^{2}S), K(5 ^{2}F) and K(5 ^{2}G) channels. Dashed vertical lines indicate channel openings. Open circles represents measured data points and solid lines numerical fits as described in the text. Vertical and horizontal lines represents the energy and width of a resonance, respectively. The thicker resonance indicators at the top of the figure are the average over the three channels. The thin resonances indicators are theoretical predictions by Liu [22].

was substantially increased to cover 3.975–4.04 eV. No previous experiments or theory have covered this energy region.

Over these two energy ranges, several partial photodetachment cross sections have been measured in K^- and Cs^- using RIS schemes equivalent to that discussed in Sec. 3.2. The observed final state channels are K(7 ^{2}S), K(5 ^{2}F), K(5 ^{2}G), Cs(10 ^{2}S), Cs(6 ^{2}F), Cs(6 ^{2}G) and Cs(6 ^{2}H). The measured cross section curves can be seen in Figs. 5.1, 5.2, and 5.3.

5.1.1 K^- Results

Two previously unobserved resonances were detected in the K(7 ^{2}S), K(5 ^{2}F) and K(5 ^{2}G) channels between the K(5 ^{2}F) and K(7 ^{2}P) channel thresholds. In

Table 5.1: Resonance parameters extracted from several measured partial cross sections of photodetachment of K^-. Resonances parameters in bold were observed in more than one channel and the arithmetic mean is thus given.

Paper **I**		Kiyan *et al.* [20]		Liu [22]	
E_r (eV)	Γ (meV)	E_r (eV)	Γ (meV)	E_r (eV)	Γ (meV)
4.28(2)	44(20)	4.292(2)	10(2)	4.275 90	–
4.294 68(9)	1.6(3)	4.2945(1)	1.5(2)	4.294 72	1.4722
–	–	4.295 76(4)	0.10(8)	4.295 803 1	0.002
4.296 21(5)	0.28(5)	4.2960(2)	0.30(3)	4.296 06	–
4.324(3)	**22(5)**	–	–	4.323 39	27.7183
4.353 02(13)	**1.72(12)**	–	–	4.353 50	–

addition, three by Kiyan *et al.* [20] previously observed resonances were detected in the $K(7\,^2S)$ channel below the $K(5\,^2F)$ threshold. A sixth, very narrow, resonance observed both by Kiyan *et al.* and calculated by Liu was not observed in the experiment in any of the three channels. This is attributed either to a small coupling between the doubly excited state and the final states investigated or the limited resolution of the experiment.

In the $K(7\,^2S)$ and $K(5\,^2F)$ channels, resonance parameters were extracted by fitting a sum of shore profiles (Eq. 2.3) and a linear background to the observed data. For the $K(5\,^2G)$ channel, a fit of two Shore profiles and the threshold law developed in Paper **III** was applied. The extracted energies and widths for all five resonances are presented in Tab. 5.1. If a resonance is observed in more than one channel the arithmetic mean of the energy and width is reported. The narrow resonance observed in the previous papers is also included for reference. The resonances observed in Paper **I**, the work by Kiyan *et al.*, and the calculations of Liu are all in good agreement.

One of the advantages of using a final state selective experimental apparatus is the ability to observe a doubly excited state in more than one final state channel. A resonances observed in more than one channel with the same energy and width, is clear evidence of the existence of a doubly excited state. In addition, the amount of resonant modulation of the non-resonant process increases with increasing final states. For example, a resonance observed in the $K(7\,^2S)$ channel

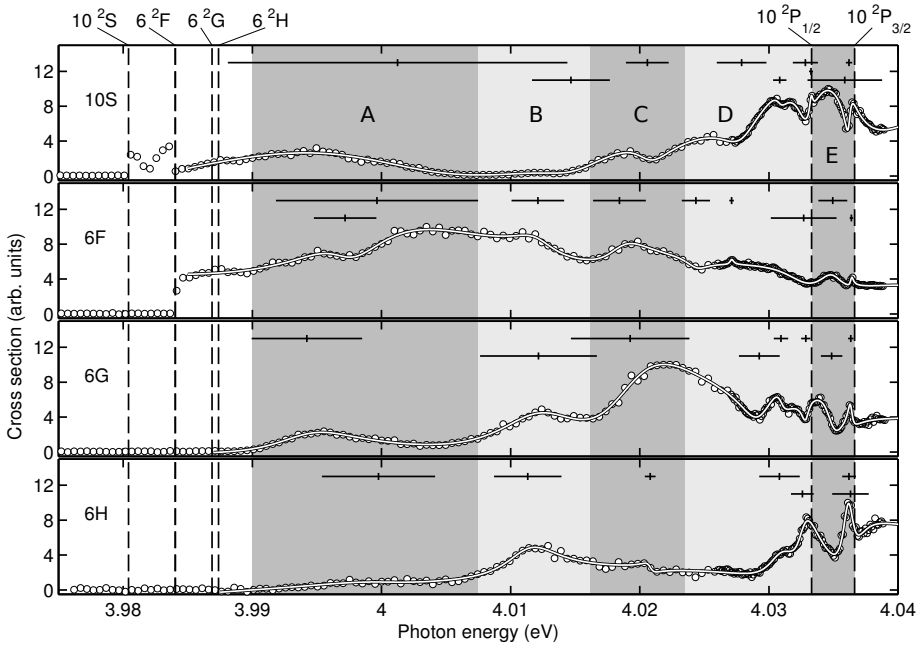

Figure 5.3: Measured cross sections for the Cs($10\,^2$S), Cs($6\,^2$F), Cs($6\,^2$G) and Na($6\,^2$H) channels. The solid lines through the data are individual fits of Eq. 5.1 to the observed data. Extracted energies and widths for the observed resonances are shown as solid vertical and horizontal lines, respectively.

modulates the cross section by approximately 90%. This is much larger than for the K($5\,^2$S) channel which Kiyan *et al.* observed, where the modulation was only 25%. Resonances that create small modulations in the cross section are harder to detect. By measuring more than one photodetachment channel, a complete picture of doubly excited states in this region is obtained.

5.1.2 Cs^- Results

The four Cs^- photodetachment spectra observed in Paper **II** are much more complicated than those observed in K^- photodetachment. In K^-, the resonances are well separated and a single Shore profile can be used for each of the resonances. In contrast, most of the resonances observed n Cs^- have large widths

and are overlapping. The overlapping resonances hinder the application of the parametrization by Shore or Fano to the resonances. In order to extract useful resonance parameters, an alternative parametrization of overlapping resonances had to be developed.

In quantum mechanics, the total transition amplitude determines the shape and magnitude of an observable cross section. In order to form the total transition amplitude, contributions from all possible paths from an initial to a final quantum state needs to be included. Each amplitude can be represented by a real number, denoted by A_i, and a complex phase shift, denoted by δ_i. Once the amplitude and phase of all the relevant paths have been worked out the total transition amplitude can be formed by the sum $T = \sum_i A_i e^{\mathrm{i}\delta_i}$. The cross section is simply the squared magnitude of the total transition amplitude.

The cross sections seen in Fig. 5.3 stems from a total transition amplitude that consists of one non-resonant direct path as well as a number of resonant paths via doubly excited states. The photodetachment process

$$\mathrm{Cs}^- + \gamma(E_\gamma) \rightarrow \mathrm{Cs}(n\ell) + e^-,$$

induced by a photon γ, represents a path carrying a transition amplitude $A_{n\ell}$ that depends on the excitation energy E_γ. We assume that the phase of this path is independent of the photon energy and use it as the definition of zero phase in order to simplify further calculations. The resonant photodetachment process

$$\mathrm{Cs}^- + \gamma(E_\gamma) \rightarrow \mathrm{Cs}^{-**}(k) \rightarrow \mathrm{Cs}(n\ell) + e^-$$

forms the rest of the contribution to the total transition amplitude. Here $\mathrm{Cs}^{-**}(k)$ indicate the k^{th} doubly excited state in Cs^- that is accessible by the energy E_γ supplied by the photon. Each of these resonant paths carry a real amplitude that consist of two parts: the Lorentz excitation profile of the doubly excited state and the branching ratio of the doubly excited state to the $\mathrm{Cs}(n\ell)$ state. The Lorentz profile is proportional to $1/\sqrt{\epsilon_k^2 + 1}$, where $\epsilon_k = (E_\gamma - E_k)/\frac{\Gamma_k}{2}$. The branching amplitude of each doubly excited state is assumed to be proportional to the non-resonant photodetachment amplitude, $A_{n\ell}$. However, the transition amplitude of different resonant paths should be independent of each other. This is taken into account by introducing a relative transition amplitude $s^k_{n\ell}$ so that the total real amplitude for one doubly excited state path is $A^k_{n\ell} = A_{n\ell} s^k_{n\ell}/(\sqrt{\epsilon_k^2 + 1})$. The phase of each resonant path has

two contributions: a constant offset, $\delta^k_{n\ell}$ and a energy-dependent phase shift, $\delta_k = \tan^{-1}(-1/\epsilon_k)$ that comes from the resonant process itself [79]. The resonant transition amplitude of the k^{th} doubly excited state then becomes

$$A^k_{n\ell} = \frac{A_{n\ell}\, s^k_{n\ell}\, e^{\mathrm{i}(\delta_k + \delta^k_{n\ell})}}{\sqrt{\epsilon_k^2 + 1}}.$$

By using the fact that $e^{\mathrm{i}\delta_k}/\sqrt{\epsilon_k^2 + 1} = 1/(\epsilon_k + \mathrm{i})$ the cross section can finally be written as

$$\sigma_{n\ell} = |T_{n\ell}|^2 = A^2_{n\ell} \left| 1 + \sum_k \frac{s^k_{n\ell}\, \mathrm{e}^{\mathrm{i}\delta^k_{n\ell}}}{\epsilon_k + \mathrm{i}} \right|^2 . \tag{5.1}$$

In the case of a single isolated resonance, one can show (see Paper **II**) that the model reduces to the Shore profile. For more than one resonance, no simple analytical form can be found. Even so, it is straightforward to implement the model in a numerical fitting routine. For k resonances, the free parameters of the model are: a linear background, $A_{n\ell}$, k $s^k_{n\ell}$ parameters, k $\delta^k_{n\ell}$ parameters and k ϵ_k parameters. The position and width of each resonance can be extracted from the corresponding ϵ_k parameter.

A large number of resonances are observed in all channels between the Cs($5\,^2$F) and Cs($10\,^2\mathrm{P}_{3/2}$) channel openings. Not every resonance is observed in all four partial cross sections. This is due to variations in branching ratios from the doubly excited state to individual cross section channels. Fits of Eq. (5.1) together with linear backgrounds to the observed cross sections data can be seen as solid lines in Fig. 5.3. Energies and widths of the resonances are marked with vertical and horizontal lines, respectively. Using the same number of resonances in all channels resulted in unstable fits. Thus, each channel has been treated separately and the fit with the least amount of resonances that could represent the data was used for resonance parameter extraction.

The doubly excited states that produce the resonances observed in the cross section have definite energies and widths. Thus, parameters extracted for the same resonance observed in several photodetachment channels should agree. From Fig. 5.3 it is apparent that the energies and widths of the resonances vary from channel to channel. This means that most assignments of doubly excited states to resonances are at best tentative. Still, since more than one photodetachment channel is used the assignments should give a good indication of the spectrum of doubly excited states that are present in the cross sections.

Figure 5.3 has been split into five parts to aid with the discussion of the observed resonances. In region A, at least two resonances are observed although only in the Cs($6\,^2$F) channel. Only one resonance is observed in region B and there is good agreement between the channels apart from a larger width in the Cs($6\,^2$G) channel. The same can be said for region C except the width of the resonance in the Cs($6\,^2$H) channel is much smaller than in the other channels. This means that most likely there are two resonances in region C. One, broad resonance, is observed in the three first channels and one, more narrow, is only observed in the Cs($6\,^2$H) channel. In region D, there are large disagreements between the channels. Nonetheless, between 4.03 eV and the Cs($10\,^2\mathrm{P}_{1/2}$) channel opening, two resonances are aligning well in the Cs($10\,^2$S), Cs($6\,^2$G) and Cs($6\,^2$H) channels. Finally, in region E just below the Cs($10\,^2\mathrm{P}_{3/2}$) channel opening there is one resonance present at the same position in all channels.

As stated before, the assignments made here are only tentative. In the end, a comparison with ab-initio calculations is needed in order to fully understand the observed cross sections.

The experiments on Cs^- shows once again the benefit of measuring more than one final state channel. In spectroscopy on bound states, the resonances observed have Lorentz profiles since the excitations can only follow a single path. A Lorentz profile carries only a positive contribution to the final cross section. Thus, it is relatively simple to observe overlapping resonances and still extract accurate information from fits to the data. In contrast, doubly excited state resonances ave both positive and negative contributions. Overlapping resonances of the Shore-type can create odd cases, e.g. it is possible to overlap two anti-symmetric resonances resulting in zero net contribution to the cross section. Thus, it is relatively difficult to draw any conclusions with only one observed final state channel. Instead, by measuring several final state channels covering the same energy region, it is possible to draw some, although tentative, conclusions about the underlying doubly excited states. This technique is shown to be effective in our experiments on Cs^-.

5.2 Threshold Behaviors

Papers **III** and **IV** presents measurements of photodetachment cross sections close to threshold of a number of highly excited final state channels in K^- and

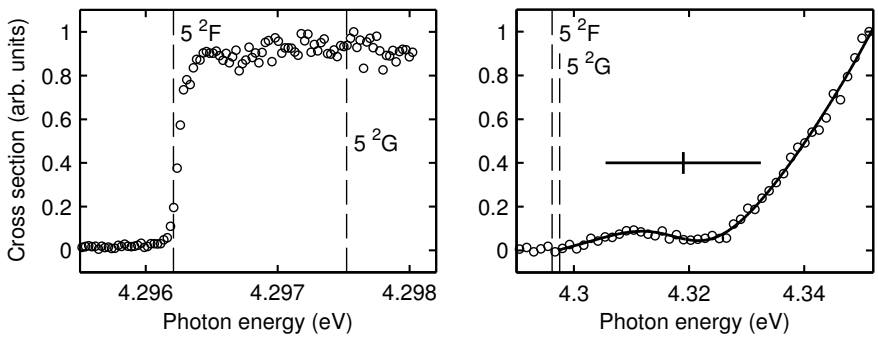

Figure 5.4: Measured cross sections for the K($5\,^2$F) and and K($5\,^2$G) channel openings. Note the large scale difference between panel (a) and (b). The solid black line in panel (b) is a fit of Eq. 5.3 and a single Shore profile to the observed data.

Na^-. In addition, the results presented in Paper **II** shown in Fig. 5.3 include several threshold observations relevant to the discussion in this section.

All three experiments show that if the photodetachment process leaves the residual atom in an excited state with a large and negative polarizability, its cross section is greatly suppressed close to threshold. This behavior had not been observed before in photodetachment experiments. In addition, all three experiments also verified that if the final state instead has a large and positive polarizability, the cross section quickly reaches a plateau. This behavior had been observed and explained before by Sandström *et al.* [80].

The first observation of the new threshold behavior was made in Paper **III** where photodetachment cross sections in the K($5\,^2$F) and K($5\,^2$G) final state channels were measured. The polarizabilities of the states have been calculated to be 3 936 137 and −3 097 696 a.u., respectively [22]. The measured cross sections can be seen in Fig. 5.4. Here it can be seen that the K($5\,^2$F) channel reaches a plateau within less than 1 meV of the threshold. The K($5\,^2$G) channel, on the other hand, is still increasing 35 meV above threshold. Due to a resonance close to threshold, there was some uncertainty as to the nature of the suppression. Although the same resonance was observed in other channels, there was a small chance that the threshold behavior was caused by the resonance itself

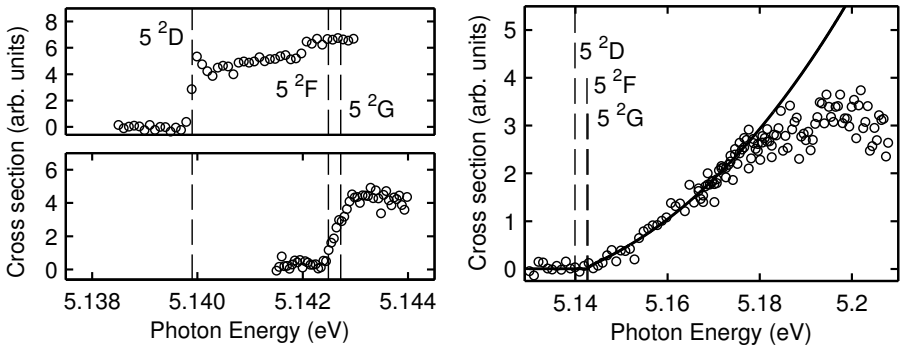

Figure 5.5: Measured cross sections for the Na($5\,^2$D), Na($5\,^2$F) and Na($5\,^2$G) channel openings. Note the large scale difference between panel (a) and (b). The solid black line in panel (b) is a fit of Eq. 5.3 to the observed data.

and not by a new threshold behavior. A continued search for a channel opening without resonances was therefore initiated. The first candidate was Cs^- and the same behavior could be verified in the $n = 6$-manifold. The polarizability of the Cs($10\,^2$S) and Cs($6\,^2$F) states are 4.75×10^5 and 7.77×10^6 a.u., respectively [81]. Unfortunately, the polarizability of the other states investigated in Cs are not known. However, they should be of the same order of magnitude as in K^-. As evident from the previous section, the many resonances in the cross section still meant that no definite verification of the new threshold behavior could be done. Finally, Na^- turned out to have just the right conditions for investigations of the new threshold behavior. The photodetachment cross section of the Na($5\,^2$F) and Na($5\,^2$G) channels, presented in Fig 5.5, show the same behavior as in K^- but without any interfering resonances. There are no measurements nor calculations of the polarizabilities of these states. Nonetheless, simple perturbation calculations give polarizabilities of 2.0×10^7 and -1.7×10^7 a.u. for the Na($5\,^2$F) and Na($5\,^2$G) states, respectively.

The results in the three papers, both for negative and positive polarizabilities, can be understood by considering the asymptotic conditions present close to a photodetachment threshold. For photodetachment to states with moderate polarizabilities, Wigner [42] realized that the effective potential is dominated by

the centrifugal term for large r (i.e. low excitations energies). In most cases, the Wigner law agrees well with observed cross sections close to threshold and it has been an extremely valuable tool in many experiments on negative ions (See e.g. Refs. [34, 43, 82, 83]). For the observations in Papers **II-IV**, the Wigner law is only valid over a very short energy range. Instead, another asymptotic limit has to be considered in order to explain the observed behavior. In these cases it is instead the polarization interaction that dominates over the centrifugal term. It should be noted that the centrifugal term will be dominating for sufficiently small values of r. The cross over point where the polarization contribution becomes larger than the centrifugal contribution has to be evaluated in order to assess if it is dominating in the energy range covered by the experiment.

For final states with large positive polarizability the observed threshold behavior can be understood by considering the outgoing electron as traveling in a strong attractive potential with a small centrifugal barrier. The height of the barrier is in the range of 10–100 μeV for the states observed in the experiments. As the excitation energy is increased above threshold, the electron is able to escape the system by tunneling through the barrier. Therefore, the cross section is seen to increase directly at threshold. As the excitation energy is increased, the probability for tunneling increases until the electron can be ejected above the barrier. At this excitation energy one would expect the cross section to flatten out. However, the outgoing electron is reflected against the barrier which reduces the probability for escape. Instead, it takes a small amount of additional excitation energy before the reflection probability is reduced to zero and the cross section levels out. This general threshold behavior can be seen in all the channels resulting in a final state with a large and positive polarizability. Even so, there are some channels that deviate from this model. One is the Na($5\,^2$F) channel which actually increases more slowly than the Na($5\,^2$D) channel even though it has a larger polarizability. The same can be seen in the Cs($6\,^2$G) channel which rises very slowly even though it is predicted to have a large positive polarizability. In order to fully describe the behavior a more complete quantum-mechanical calculation is needed. This was performed by Wantabe and Greene [84], who created a modified effective range theory that explained photodetachment threshold behaviors observed in photodetachment to final states with large and positive polarizabilities in Li^- and K^- [80].

For states with large and negative polarizability, the outgoing electron is

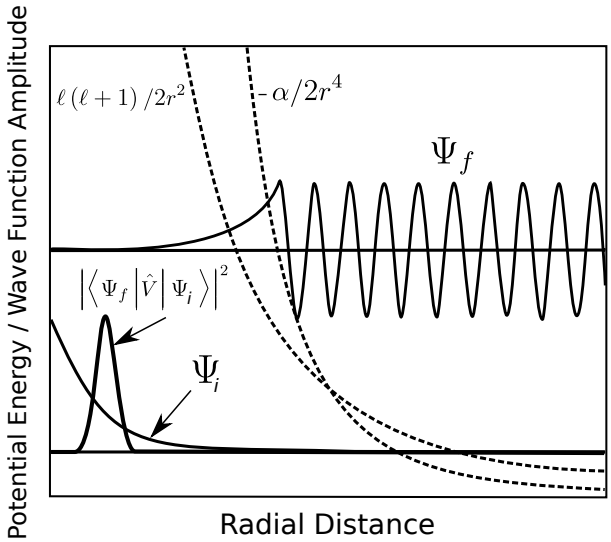

Figure 5.6: A schematic overview of the potentials and wave functions involved in the derivation of the new threshold model contained in Eq. 5.3

instead traveling in a strictly repulsive potential. Nonetheless, for sufficiently large r, the Wigner law should still be valid. In the case of photodetachment to the Na($5\,^2$G) channel, the cross over point where the polarization potential starts to dominate is approximately at $r = 1200$ a.u.. This radial distance translates into an energy above threshold of 0.23 meV, which means that the resolution of the experiment cannot resolve the energy region where the Wigner law is expected to be valid. It also means that we can assume for the further discussion that the polarization interaction is the only one that affects the shape of the cross section near threshold that we observe in the experiments.

In Paper **III**, a new threshold law was developed under the assumptions mentioned above. A sketch describing the model can be seen in Fig. 5.6. The general idea is to find analytical forms of the initial and final state wave functions of the detaching electron. The observed cross section is then simply the overlap of these two wave functions. The initial wave function can be approximated by Hartree-Fock wave functions from standard tables [85]. The continuum wave function, on the other hand, is made up of two parts: a plane wave in the classically allowed region and an exponential tail in the classically forbidden region. The two parts of the outgoing wave function can be found by using the

semi-classical WKB-approximation. Here, the de Broglie wavelength is assumed to be much smaller than the size of the typical length scale of the system. This is true for most unbound electron motion except at classical turning points where the wavelength goes to infinity. In our case, the only part of the wave function that is of interest is the one where the initial and final wave functions overlap. The initial state wave functions only protrude a few Bohr radii from the nucleus. Therefore, the two wave functions only overlap in a narrow region close to the nucleus. The classical turning point for an energy above threshold of 30 meV is $r_0 = 300$ a.u. which is far from the region where the two wave functions interact. Thus, the WKB-approximation will be valid in this case. Once the wave functions have been calculated, the shape of the cross sections can be calculated from the following expression (atomic units):

$$\sigma \propto \int_k \left| \left\langle \Psi_f \left| \hat{V} \right| \Psi_i \right\rangle \right|^2 \delta \left(E + E_a + E_i - E_\gamma \right) \frac{\mathrm{d}^3 \mathbf{k}}{(2\pi)^3}. \tag{5.2}$$

Here, E is the energy of the outgoing electron, $\hat{V}$ denotes the transition operator, $|\Psi_f\rangle$ and $|\Psi_i\rangle$ the final and initial state wave functions, E_i is the initial state energy, E_a is the energy of the residual atom, and E_γ is the photon energy. Integrating the above expression using the correct wave functions yields a very simple threshold law

$$\sigma \propto \exp\left[D E^{\frac{1}{4}} \right], \tag{5.3}$$

where $D = 2.396(2|\alpha|)^{1/4}$. The only free parameters in the model are the threshold position and the polarizability α of the final state.

In Fig. 5.5b a fit of the model to the cross section data can be seen as the solid line. The model fits the data well up to 35 meV where the cross section starts to level out. At higher energies, it is most likely that the electron wave function has started to penetrate so far that the interactions no longer can be described by a simple dipole polarization interaction. Instead, a more complete electron correlation interaction would be needed together with a full quantum-mechanical calculation. Nonetheless, the new model adequately describes the observed threshold behavior.

In principal, the model should allow us to extract a dipole polarizability of the final state from the fitted value of D. In the case of both the K($5\,^2$G) and Na($5\,^2$G) final state the extracted value of α is two to three orders of magnitude too small but it does give a polarizability that is much larger compared to most

atomic states. It is not very surprising that the model cannot give quantitative results since it has been developed using simple approximations. In order to fully describe the system, a full ab-initio quantum mechanical calculation is needed.

Both the experiments on K^- and Na^- shows the flexibility of the state selective detection that is possible at GUNILLA. Firstly, it enabled us to detect the different threshold behaviours. Secondly, by observing the interfering resonance in the K($5\,^2$G) channel in more than one partial cross section, we could conclude that the shape of the cross section was not only due to the resonance but had to come from a new threshold behavior.

5.3 Design of a Field Ionizer for Studies of Negative Ions

The new field ionizer setup that is the topic of Paper **V** has been described in detail in Sec. 4.3. In summary, a new field ionizer consisting of 12 coaxial circular plates can be used to tailor the electric field necessary for studies of the photodetachment process. Three experimental scenarios are simulated and the performance of each case is evaluated.

In order to test the new setup, a trial experiment on Cs^-has been performed. The ground state configuration of Cs and Cs^- is $6s$ and $6s^2$, respectively. Thus, photodetachment to the ground state in Cs will result in p-wave photodetachment. This reduces the accuracy on the determination of the EA of Cs. Until now, the most accurate published EA comes from a measurement to the ground state [75]. There exists a more accurate measurement of the EA of Cs, but it has only been tabulated in the review by Hotop and Lineberger in 1985 [86]. Therefore, the first test of the new setup will be to measure the EA of Cs by detecting a final state channel with s-wave behavior.

With the lasers available at GUNILLA, the lowest lying accessible final state channel that results in s-wave photodetachment is Cs($8\,^2$P). Unfortunately, the PSD was broken during the final time-window open for experiments. It was therefore replaced with a small aperture channeltron setup. This reduced the diagnostic abilities during the experiment and it was not possible to detect the signal of this final state channel. To prove the RIS part of the design, we instead measured the ground state photodetachment channel. Here, IR photons are used for photodetachment while the UV photons resonantly excites the Cs($6\,^2$S) $\rightarrow$

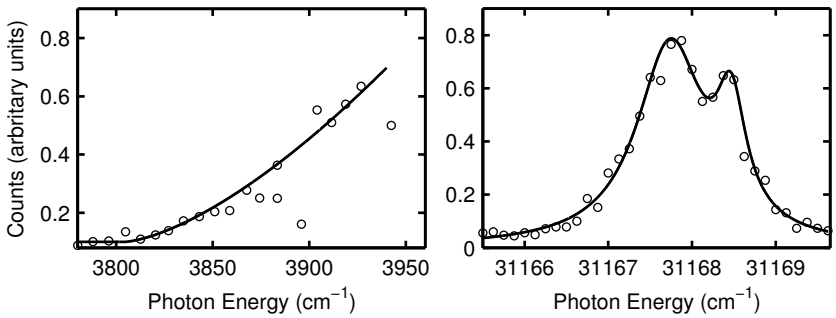

(a) **(b)**

Figure 5.7: Results from first experiments using the new detection system described in Sec. 4.3. (a) shows photodetachment cross section measurements to the grounds state of Cs. (b) shows a scan over two resonant transition from the ground state to the $25\,^2\mathrm{P}_{1/2,\,3/2}$ states. The solid lines represent a fit of the Wigner law and two Lorentz profiles to the data in (a) and (b), respectively.

Cs($25\,^2$P) transition. The resulting Cs Rydberg atoms are field ionized by a field similar to that described in Sec. 4.3.1. The resulting cross section curve can be seen in Fig. 5.7a. Although the data needs to be improved it is clear that we observe a p-wave threshold corresponding to ground state photodetachment.

In order to show that we indeed are observing signal stemming from field ionized Rydberg atoms, the UV photon energy is scanned over the two fine structure components of the Cs($25\,^2$P) configuration. This results in two Lorentz resonance peaks that can be seen in Fig. 5.7b. The extracted positions of the two resonances are 31 167.74(4) and 31 168.47(3) cm^{-1}, respectively. This should be compared with the previously measured positions of the Cs($25\,^2$P) states of 31 167.01727(15) and 31 167.74257(20) cm^{-1}, respectively [87]. The splitting of the two states are in good agreement but there is a shift of approximately 0.7 cm^{-1} of the new measurement compared to the older measurements. This shift corresponds to 3.5 bandwidths of the laser. Most likely, the shift is the result of an uncalibrated wavelength meter. However, this uncertainty is sufficient for the purpose of RIS, since we unambiguously can identify the transition lines. The current data shows that the apparatus is performing within expectations and once the PSD is repaired, it is expected to significantly enhance the capabilities

of GUNILLA.

5.4 Bound States of Opposite Parity in La^-

Bound excited states with a parity opposite that of the ground state are indeed a rarity among negative ions. The shallow potential that binds the outer electrons are usually too week to bind more than hyperfine, fine and occasionally term splitting states of the the ground state electron configuration. Since these states have the same parity, no allowed optical transitions are observed in most negative ions. Up until now, only Ce^-, and Os^- have been observed to have bound states of opposite parity [36, 40].

Negative ions with bound states of opposite parity are interesting in themselves since it is the especially strong electron correlation that permit the dense structure of excited states. More interestingly, such negative ions should be possible to laser cool. Laser cooled negative ions could then be used to sympathetically cool other negatively charged systems. This would for example open up the possibility to cool anti-protons with the prospect to enhance the production of anti-hydrogen.

Unfortunately, Ce^- and Os^- have been proved to be unfavorable for laser cooling due to the need for re-pumping of dark states and a relatively low strength of the proposed cooling transition [88]. Luckily, there are more negative ions proposed to have bound states with opposite parity with respect to the ground state. In particular, the negative ion of lanthanum, La^-, is now expected to be a better candidate for laser cooling applications. Theoretical studies by O'Malley and Beck [41, 89], show that La^- should have seven even ($[Xe]5d^26s^2$) and eight odd ($[Xe]5d6s^26p$) parity states. A number of optically allowed transitions involving $6p \leftrightarrow 5d$ excitations should thus exist. In particular, the transition from the $^3F_2^e$ ground state to the $^3D_1^o$ excited states showed promising properties for laser cooling.

Paper **VI** describes an experimental survey of the bound states of La^-. The experiment was performed at the Department of Physics at Denison University. In the experiment, a ns pulsed tunable infrared laser was overlapped perpendicularly to a 12 keV ion beam of La^-. Any photodetached La^- was separated from the negative ion beam and detected in the forward direction. The laser delivered pulses with photon energies ranging from 260 to 539 meV.

Table 5.2: Observed bound-bound transitions in La^-. The transition in bold is the proposed laser cooling transition.

Transition	Experiment Energy (meV)	Experiment Width (meV)	Calculated Energy (meV)	Calculated A coeff. (s^{-1})
$^3F_3^e \rightarrow {}^3F_2^o$	259.76(4)	–	192	260
$^3F_3^e \rightarrow {}^3F_3^o$	299.94(3)	0.016(6)	238	900
$^3F_4^e \rightarrow {}^3F_4^o$	323.33(3)	0.025(6)	271	1700
$^3F_2^e \rightarrow {}^3F_2^o$	343.69(3)	0.014(6)	259	530
$^3F_4^e \rightarrow {}^3D_3^o$	365.94(3)	0.19(4)	326	31 000
$^3F_2^e \rightarrow {}^3F_3^o$	383.87(3)	0.021(6)	305	1600
$^3F_3^e \rightarrow {}^3D_2^o$	386.59(4)	0.24(7)	329	26 000
$\mathbf{^3F_2^e \rightarrow {}^3D_1^o}$	**399.42(3)**	**0.28(3)**	**337**	**29 000**
$^3F_3^e \rightarrow {}^3F_4^o$	412.24(3)	0.020(4)	339	150
$^3F_3^e \rightarrow {}^3D_3^o$	454.86(3)	0.021(6)	394	1800
$^3F_2^e \rightarrow {}^3D_2^o$	470.55(3)	0.032(8)	396	3600
$^3F_2^e \rightarrow {}^3D_3^o$	538.80(3)	0.016(6)	461	21

The EA of La^- has been measured and calculated to be 470(20) [90] and 545 meV [89], respectively. As the energy of the laser was scanned, 12 narrow peaks were observed in the photodetachment spectrum. Since the excitation energies for most of these peaks are lower than the EA of La^-, they can only be the result of bound-bound transitions followed by photodetachment from the excited state. By using repetitive features of the 12 peaks, it was possible to uniquely define the location of eight excited states in La^-. A list of the 12 observed transitions together with state assignments, transitions energies and widths can be found in Tab. 5.2. Transitions involving six out of the 15 predicted states were not seen since they were not accessible from the states populated by the ion source.

The results obtained in the experiment are very promising for future applications of laser cooling. An optimal laser cooling system should only contain a single transition with a large transition amplitude. Such a systems would not need re-pumping of dark states and should allow for a relatively low-power laser to efficiently cool the ions. These first results show that La^- might provide such a system. The $^3F_2^e \rightarrow {}^3D_1^o$ transition is the only one involving the $^3D_1^o$ state. This is a good indication that it is not connected to any other state than the

ground state via dipole transitions, thus forming an effective two level system. In addition, the observed width of the peak in the experiment was seen to be large when compared to most of the other transitions. Most likely, this is due to power broadening of the peak, indicating that it indeed is a strong transition, which is also supported by calculations [41].

In summary, La^- is the most promising candidate for a demonstration of laser cooling of negative ions. The main drawback is the modest 30 pA of ion current that is achievable with existing ion sources. However, the long loading times of ion traps due to few collisional losses should permit a large density of trapped La^- ions. In addition, there is little need for cooling of the ion beam prior to trapping which also simplifies the procedure.

6

Conclusion & Outlook

In this thesis a number of photodetachment experiments have been performed using the GUNILLA apparatus. The results have led to a significant increase in our knowledge of the structure and dynamics of negative ions. All the experiments have involved photodetachment to highly excited states of the residual parent atom, thus probing highly correlated, yet simple, atomic systems.

I consider the observation of a new threshold behavior for final state channels with a large negative polarizability as the most important result. We now have a solid understanding of the phenomena and the fact that we have observed the behavior in three separate systems strengthens the confirmation of the observed process. Interestingly, the observed threshold behaviors are very similar to that of β-decay [91]. In both β^--decay and photodetachment to a final state of large and positive polarizability the cross section for the processes are seen to increase rapidly just above threshold. In contrast, the cross section near threshold for both β^+-decay and photodetachment to a final state with large and negative polarizability are seen to increase much more slowly. Even tough β-decay and photodetachment are very different processes they both present the same underlying situation of an electron moving in either a strong attractive or repulsive potential. In the case of the repulsive potential, the electron is brought into the forbidden region of the potential and has to "tunnel out" in order to be emitted. It is this tunneling that is responsible for the observed suppression of the two processes. The process of photodetachment to final states with high polarizability and β-decay thus represents an excellent example of the universality of

physics.

The photodetachment experiments on K^- and Cs^- have substantially increased the amount of information on measured partial cross sections for the two systems. In total, partial cross sections for eight new photodetachment channels were recorded. In addition, we observed many resonances in the cross sections due to the auto-ionizing decay of doubly excited states. In the case of K^-, five doubly excited states were found. Two of these had not been observed previously. For Cs^-photodetachment, we observed a large amount of doubly excited state resonances. Many of these resonances were overlapping, thus excluding the use of the Fano or Shore parametrization in the extraction of the resonance parameters. As a result, it was necessary to develop an alternative resonance parametrization in order to determine the energy and width of the resonances. State selective detection using RIS have been proven to be a valuable tool in the interpretation of the observed resonance structure. By using more than one photodetachment channel, one is ensured that no resonances are missed due to a weak signal arising from inadequate coupling between a doubly excited state and a specific photodetachment channel. In the case of Cs^-, measurements of more than one photodetachment channel were essential for the interpretation of the complex resonance structure.

The experiments on both the threshold behavior and the doubly excited states leaves room for theoretical input. The semi-classical model developed to explain the behavior for the new threshold behavior does not provide quantitative results. Clearly a quantum mechanical calculation that includes electron correlation is needed. The rich spectrum of doubly excited states in Cs^- that was observed presents a formidable challenge at the theoretical level. I hope therefore that the work presented in this thesis will attract the attention of new theoretical input in order to formulate a quantum mechanical model for these systems.

Future prospects for investigations at the collinear setup at GUNILLA is summarized in the section on the design of the new field ionizer setup. Although the old arrangement was efficient, it had several drawbacks that hindered further investigations of photodetachment to even more highly excited states of the residual atom. The new design incorporates a collinear field ionizer and a separate energy analyzer. With this field ionizer, almost any electric field profile can be realized. It should allow a new range of experiments to be performed

involving excitation energies extending up to and beyond the double detachment limit. In particular, two new types of photodetachment experiments can be performed. One is the investigation of branching ratios to highly excited Rydberg states of the residual atom and the other is to investigate the double detachment process in which two electrons are simultaneously detached from a negative ion. Hopefully, the new experimental design will finally enable future measurements to shed light on these fundamental problems.

In addition to the work performed at GUNILLA in Sweden, I have been involved in measurements on twelve optical transitions between bound states of opposite parity in La^-. The experiment was performed at the Dension University in the USA. The results confirm that La^- is only the third negative ion found to have bound states of opposite parity. By using patterns among the observed transitions, all the lower and upper states involved were identified. The transition between the $^3F_2^e$ ground state to the excited $^3D_1^o$ state should be particularly well suited for a recently proposed laser cooling scheme. Calculations show that the upper state almost exclusively decays back to the ground state. In addition, both experiment and theory indicate that the transition strength is strong. This supports the predictions that La^- could be very efficiently laser cooled. If this is possible, it would open up a sympathetic cooling mechanism that could be applied to most negatively charged particles. The most interesting prospect would be to cool anti-protons in an effort to enhance anti-hydrogen production. However, before any laser cooling can be undertaken, more precise measurements of branching ratios and transition intensities in La^- are needed.

Acknowledgment

Table 6.1: Recipients of gratitude.

Recipient	Motivation
Dag Hanstorp	For guidance and pep talks whenever I needed them. And for showing that academia is so much more than just research.
Anton Lindahl Pontus Andersson Peter Klason Hannes Hultgren Mikael Eklund Oscar Isaksson Olle Windelius Tobias Leopold	For all the discussions about physics both in an out of the lab. And for the great sense of belonging that you all have helped to create.
Ann-Marie Pendrill	For the teaching perspective and for all the Liseberg physics opportunities.
Mats Rostedt	For being a helping hand with all things technical and electrical in the lab.
Jan-Åke Wiman	Probably the best instrument maker in the world.
David Pegg Jonas Einarsson	For improving the quality of this thesis.
All past and present Level 8 Colleagues	For producing a stimulating work environment and for all the interesting discussions about science and everything else in the lunch room and Friday Cake sessions.
Erik Werner	For this table acknowledgment format [92].
Friends and family	For your company, support and love.
Elisabet	For love, love and love.

References

[1] J. J. Thomson. **Bakerian Lecture: Rays of Positive Electricity**. *Proceedings of the Royal Society A: Mathematical, Physical and Engineering Sciences*, **89**:1–20, 1913.

[2] R. Wildt. **Negative Ions of Hydrogen and the Opacity of Stellar Atmospheres.** *The Astrophysical Journal*, **90**:611–620, 1939.

[3] L. M. Branscomb and S. J. Smith. **Experimental Cross Section for Photodetachment of Electrons from H^- and D^-**. *Physical Review*, **258**:1028–1034, 1955.

[4] D. S. Burch, S. J. Smith, and L. M. Branscomb. **Photodetachment of O_2^-**. *Physical Review*, **183**:171–175, 1957.

[5] L. M. Branscomb, D. S. Burch, S. J. Smith, and S. Geltman. **Photodetachment Cross Section and the Electron Affinity of Atomic Oxygen**. *Physical Review*, **922**:504–513, 1958.

[6] M. L. Seman and L. M. Branscomb. **Structure and Photodetachment Spectrum of the Atomic Carbon Negative Ion**. *Physical Review*, **258**:1602–1608, 1962.

[7] H. S. W. Massey. *Negative Ions*. Cambridge University Press, New York, 3rd edition, 1976.

[8] T. Andersen. **Atomic Negative Ions: Structure, Dynamics and Collisions**. *Physics Reports*, **394**:157–313, 2004.

[9] D. J. Pegg. **Structure and Dynamics of Negative Ions**. *Reports on Progress in Physics*, **67**:857–905, 2004.

[10] T. Andersen, H. K. Haugen, and H. Hotop. **Binding Energies in Atomic Negative Ions: III**. *Journal of Physical and Chemical Reference Data*, **28**:1511–1533, 1999.

[11] J. C. Rienstra-Kiracofe, G. S. Tschumper, H. F. Schaefer, S. Nandi, and G. B. Ellison. **Atomic and Molecular Electron Affinities: Photoelectron Experiments and Theoretical Computations.** *Chemical reviews*, **102**:231–282, 2002.

[12] G. Tanner, K. Richter, and J.-M. Rost. **The Theory of Two-Electron Atoms: Between Ground State and Complete Fragmentation**. *Reviews of Modern Physics*, **72**:497–544, 2000.

[13] R. P. Madden and K. Codling. **New Autoionizing Atomic Energy Levels in He, Ne, and Ar**. *Physical Review Letters*, **10**:10–13, 1963.

[14] M. Domke, C. Xue, A. Puschmann, T. Mandel, E. Hudson, D. A. Shirley, G. Kaindl, C. H. Greene, H. R. Sadeghpour, and H. Petersen. **Extensive Double-Excitation States in Atomic Helium**. *Physical Review Letters*, **66**:1306–1309, 1991.

[15] P. G. Harris, H. C. Bryant, A. H. Mohagheghi, R. A. Reeder, C. Y. Tang, J. B. Donahue, and C. R. Quick. **Observation of Doubly Excited Resonances in the H^- Ion**. *Physical Review A*, **42**:6443–6465, 1990.

[16] P. G. Harris, H. C. Bryant, A. H. Mohagheghi, R. A. Reeder, H. Sharifan, C. Y. Tang, H. Tootoonchi, J. B. Donahue, C. R. Quick, D. C. Rislove, W. W. Smith, and J. E. Stewart. **Observation of High-Lying Resonances in the H^- Ion**. *Physical Review Letters*, **65**:309–312, 1990.

[17] H. R. Sadeghpour and C. H. Greene. **Dominant Photodetachment Channels in H^-**. *Physical Review Letters*, **65**:313–316, 1990.

[18] P. Camus, T. F. Gallagher, J.-M. Lecomte, P. Pillet, L. Pruvost, and J. Boulmer. **Observation of an Electronic Correlation for Double-Rydberg States of Barium**. *Physical Review Letters*, **62**:2365–2368, 1989.

[19] G. Haeffler, I. Yu. Kiyan, D. Hanstorp, B. J. Davies, and D. J. Pegg. **Observation of Resonance Structure in the Na^- Photodetachment Cross Section**. *Physical Review A*, **59**:3655–3659, 1999.

[20] I. Yu. Kiyan, U. Berzinsh, J. Sandström, and D. J. Pegg. **Spectrum of Doubly Excited States in the K^- Ion**. *Physical Review Letters*, **84**:5979–5982, 2000.

[21] G. Haeffler, I. Yu. Kiyan, U. Berzinsh, D. Hanstorp, N. Brandefelt, E. Lindroth, and D. J. Pegg. **Strongly Correlated States in the Li^- Ion**. *Physical Review A*, **63**:053409, 2001.

[22] C.-N. Liu. **Photodetachment of K^-**. *Physical Review A*, **64**:052715, 2001.

[23] E. Lindroth and J. Luis Sanz-Vicario. **Photodetachment of Few-Electron Negative Ions**. *Radiation Physics and Chemistry*, **70**:387–405, 2004.

[24] E. Herbst and W. Klemperer. **The Formation and Depletion of Molecules in Dense Interstellar clouds**. *The Astrophysical Journal*, **185**:505–533, 1973.

[25] E. Herbst. **Can Negative Molecular Ions be Detected in Dense Interstellar Clouds?** *Nature*, **289**:656–657, 1981.

[26] M. C. McCarthy, C. A. Gottlieb, H. Gupta, and P. Thaddeus. **Laboratory and Astronomical Identification of the Negative Molecular ion C_6H^-**. *The Astrophysical Journal*, **652**:L141–L144, 2006.

[27] E. Herbst. **Negative Ions in Space: What They Are Telling Us**. *ASP Conference Series*, **417**:153–164, 2009.

[28] A. G. G. M. Tielens. **The Molecular Universe**. *Reviews of Modern Physics*, **85**:1021–1081, 2013.

[29] C. L. Bennett, R. P. Beukens, and M. R. Clover. **Radiocarbon Dating Using Electrostatic Accelerators: Negative Ions Provide the Key**. *Science*, **198**:508–510, 1977.

[30] D. E. Nelson, R. G. Korteling, and W. R. Stott. **Carbon-14: Direct Detection at Natural Concentrations**. *Science*, **198**:507–508, 1977.

[31] W. Kutschera. **Progress in Isotope Analysis at Ultra-Trace Level by AMS**. *International Journal of Mass Spectrometry*, **242**:145–160, 2005.

[32] R. Hemsworth, H. Decamps, J. Graceffa, B. Schunke, M. Tanaka, M. Dremel, A. Tanga, H. P. L. De Esch, F. Geli, J. Milnes, T. Inoue, D. Marcuzzi, P. Sonato, and P. Zaccaria. **Status of the ITER Heating Neutral Beam System**. *Nuclear Fusion*, **49**:045006, 2009.

[33] J. E. Sansonetti and W. C. Martin. **Handbook of Basic Atomic Spectroscopic Data**. *Journal of Physical and Chemical Reference Data*, **34**:1559–2259, 2005.

[34] P. Andersson, A. O. Lindahl, C. Alfredsson, L. Rogström, C. Diehl, D. J. Pegg, and D. Hanstorp. **The Electron Affinity of Phosphorus**. *Journal of Physics B: Atomic, Molecular and Optical Physics*, **40**:4097–4107, 2007.

[35] M. Scheer, R. C. Bilodeau, C. A. Brodie, and H. K. Haugen. **Systematic Study of the Stable States of C^-, Si^-, Ge^-, and Sn^- via Infrared Laser Spectroscopy**. *Physical Review A*, **58**:2844–2856, 1998.

[36] R. C. Bilodeau and H. K. Haugen. **Experimental Studies of Os^-: Observation of a Bound-Bound Electric Dipole Transition in an Atomic Negative Ion**. *Physical review letters*, **85**:534–537, 2000.

[37] U. Warring, M. Amoretti, C. Canali, A. Fischer, R. Heyne, J. Meier, Ch. Morhard, and A. Kellerbauer. **High-Resolution Laser Spectroscopy on the Negative Osmium Ion**. *Physical Review Letters*, **102**:043001, 2009.

[38] A. Fischer, C. Canali, U. Warring, A. Kellerbauer, and S. Fritzsche. **First Optical Hyperfine Structure Measurement in an Atomic Anion**. *Physical Review Letters*, **104**:073004, 2010.

[39] C. W. Walter, N. D. Gibson, C. M. Janczak, K. A. Starr, A. P. Snedden, R. L. Field III, and P. Andersson. **Infrared Photodetachment of Ce^-: Threshold Spectroscopy and Resonance Structure**. *Physical Review A*, **76**:052702, 2007.

[40] C. W. Walter, N. D. Gibson, Y.-G. Li, D. J. Matyas, R. M. Alton, S. E. Lou, R. L. Field III, D. Hanstorp, L. Pan, and D. R. Beck. **Experimental and Theoretical Study of Bound and Quasibound States of Ce^-**. *Physical Review A*, **84**:032514, 2011.

[41] S. M. O'Malley and D. R. Beck. **Lifetimes and Branching Ratios of Excited States in La^-, Os^-, Lu^-, Lr^-, and Pr^-**. *Physical Review A*, **81**:032503, 2010.

[42] E. P. Wigner. **On the Behavior of Cross Sections Near Thresholds**. *Physical Review*, **73**:1002–1009, 1948.

[43] R. C. Bilodeau, M. Scheer, H. K. Haugen, and R. L. Brooks. **Near-Threshold Laser Spectroscopy of Iridium and Platinum Negative ions: Electron Affinities and the Threshold Law**. *Physical Review A*, **61**:1–7, 1999.

[44] T. F. O'Malley. **Effect of Long-Range Final-State Forces on the Negative-Ion Photodetachment Cross Section Near Threshold**. *Physical Review*, **75**:1668–1672, 1965.

[45] J. W. Farley. **Photodetachment Cross Sections of Negative Ions: The Range of Validity of the Wigner Threshold Law**. *Physical Review A*, **40**:6288–6292, 1989.

[46] U. Fano. **Effects of Configuration Interaction on Intensities and Phase Shifts**. *Physical Review*, **124**:1866–1878, 1961.

[47] B. W. Shore. **Analysis of Absorption Profiles of Autoionizing Lines**. *Journal of The Optical Society of America*, **57**:881–884, 1967.

[48] P. Balling, H. H. Andersen, and C. A. Brodie. **High-Resolution VUV Spectroscopy of H^- in the Region Near the $H(n = 2)$ Threshold**. *Physical Review A*, **61**:9–11, 2000.

[49] H. R. Sadeghpour, J. L. Bohn, M. J. Cavagnero, B. D. Esry, I. I. Fabrikant, J. H. Macek, and A. R. P. Rau. **Collisions Near Threshold in Atomic and Molecular Physics**. *Journal of Physics B: Atomic, Molecular and Optical Physics*, **33**:R93–R140, 2000.

[50] S. I. Themelis. **Wannier-Ridge States of He and H^- With Symmetries $^3P^e$ and $^1D^o$ and the Validity of Classification Schemata.** *The Journal of chemical physics*, **132**:154111, 2010.

[51] T. A. Patterson and H. Hotop. **Resonances in Alkali Negative-Ion Photodetachment and Electron Affinities of the Corresponding Neutrals**. *Physical Review Letters*, **5012**:189–192, 1974.

[52] P. Frey, F. Breyer, and H. Hotop. **High Resolution Photodetachment from the Rubidium Negative Ion Around the Rb($5p_{1/2}$) Threshold**. *Journal of Physics B: Atomic and Molecular Physics*, **11**:589–594, 1978.

[53] J. Slater, F. H. Read, S. E. Novick, and W. C. Lineberger. **Alkali Negative Ions. III. Multichannel Photodetachment Study of Cs^- and K^-**. *Physical Review A*, **17**:201–213, 1978.

[54] U. Ljungblad, D. Hanstorp, U. Berzinsh, and D. J. Pegg. **Observation of Doubly Excited States in Li^-**. *Physical Review Letters*, **77**:3751–3754, 1996.

[55] G. S. Hurst, M. G. Payne, M. H. Nayfeh, J. P. Judish, and E. B. Wagner. **Saturated Two-Photon Resonance Ionization of He(2^1S)**. *Physical Review Letters*, **35**:82–85, 1975.

[56] G. S. Hurst and M. G. Payne. *Principles and Applications of Resonance Ionization Spectroscopy*. IOP Publishing Ltd, Philapelphia, 1988.

[57] G. S. Hurst, M. G. Payne, S. D. Kramer, and J. P. Young. **Resonance Ionization Spectroscopy and One-Atom Detection**. *Reviews of Modern Physics*, **51**:767–816, 1979.

[58] S. Rothe, A. N. Andreyev, S. Antalic, A. Borschevsky, L. Capponi, T. E. Cocolios, H. De Witte, E. Eliav, D. V. Fedorov, V. N. Fedosseev, D. A. Fink, S. Fritzsche, L. Ghys, M. Huyse, N. Imai, U. Kaldor, Y. Kudryavtsev, U. Köster, J. F. W. Lane, J. Lassen, V. Liberati, K. M. Lynch, B. A. Marsh, K. Nishio, D. Pauwels, V. Pershina, L. Popescu, T. J. Procter, D. Radulov, S. Raeder, M. M. Rajabali, E. Rapisarda, R. E. Rossel, K. Sandhu, M. D. Seliverstov, A. M. Sjödin, P. Van den Bergh, P. Van Duppen, M. Venhart, Y. Wakabayashi, and K. D. A. Wendt. **Measurement of the First Ionization Potential of Astatine by Laser Ionization Spectroscopy.** *Nature communications*, **4**:1835, 2013.

[59] V. N. Fedoseyev, G. Huber, U. Köster, J. Lettry, V. I. Mishin, H. Ravn, V. Sebastian, and ISOLDE Collaboration. **The ISOLDE Laser Ion Source for Exotic Nuclei**. *Hyperfine Interactions*, **127**:409–416, 2000.

[60] E. Kugler. **The ISOLDE Facility**. *Hyperfine Interactions*, **129**:23–42, 2000.

[61] J. E. Bayfield and P. M. Koch. **Multiphoton Ionization of Highly Excited Hydrogen Atoms**. *Physical Review Letters*, **33**:258–261, 1974.

[62] C. E. Theodosiou. **Lifetimes of Alkali-Metal–Atom Rydberg States**. *Physical Review A*, **30**:2881–2909, 1984.

[63] C. Diehl, K. Wendt, A. O. Lindahl, P. Andersson, and D. Hanstorp. **Ion Optical Design of a Collinear Laser-Negative Ion Beam Apparatus**. *Review of Scientific Instruments*, **82**:053302, 2011.

[64] P. Defrance, F. Brouillard, W. Claeys, and G. van Wassenhove. **Crossed Beam Measurement of Absolute Cross sections : an Alternative Method and its Application to the Electron Impact Ionisation of He^+**. *Journal of Physics B: Atomic, Molecular and Optical Physics*, **14**:103–110, 1984.

[65] T. Leopold, J. Rohlén, P. Andersson, C. Diehl, M. Eklund, O. Forstner, D. Hanstorp, H. Hultgren, P. Klason, A. O. Lindahl, and K. Wendt. **Feasibility of Photodetachment Isobar Suppression of WF With Respect to HfF**. *International Journal of Mass Spectrometry*, **359**:12–18, 2014.

[66] R. Middleton. **A Versatile High Intensity Negative Ion Source**. *Nuclear Instruments and Methods in Physics Research*, **214**:139–150, 1983.

[67] J. Heinemeier and P. Hvelplund. **Production of 15-90 keV Negative Heavy Ions by Charge Exchange With Mg Vapour**. *Nuclear Instruments and Methods*, **148**:65–75, 1977.

[68] J. Heinemeier and P. Hvelplund. **Production of 10–80 keV Negative Heavy Ions by Charge Exchange in Na Vapour**. *Nuclear Instruments and Methods*, **148**:425–429, 1978.

[69] S. L. Kaufman. **High-Resolution Laser Spectroscopy in Fast Beams**. *Optics Communications*, **17**:309–312, 1976.

[70] K. Stratmann, R. Hohmann, H.-J. Kluge, S. Kunze, J. Lantzsch, L. Monz, E. W. Otten, G. Passler, J. Stenner, K. Wendt, and K. Zimmer. **High-Resolution Field Ionizer for State-Selective Detection of Rydberg Atoms in Fast-Beam Laser Spectroscopy**. *Review of Scientific Instruments*, **65**:1847–1852, 1994.

[71] G. H. Wannier. **The Threshold Law for Single Ionization of Atoms or Ions by Electrons**. *Physical Review*, **90**:817–825, 1953.

[72] A. Temkin. **The Energy Distribution Cross Section in Threshold Electron-Atom Impact Ionization**. *Journal of Physics B: Atomic and Molecular Physics*, **7**:L450–L453, 1974.

[73] J. B. Donahue, P. A. M. Gram, M. V. Hynes, R. W. Hamm, C. A. Frost, H. C. Bryant, K. B. Butterfield, D. A. Clark, and W. W. Smith. **Observation of Two-Electron Photoionization of the H- Ion near Threshold**. *Physical Review Letters*, **48**:1538–1541, 1982.

[74] Y. K. Bae and J. R. Peterson. **Near-Threshold Measurments of K- Two-Electron Photoionization Cross Sections**. *Physical Review A*, **37**:3254–3258, 1988.

[75] M. Scheer, J. Thø gersen, R. C. Bilodeau, C. A. Brodie, and H. K. Haugen. **Experimental Evidence that the $6s6p^3P_J$ States of Cs^- Are Shape Resonances**. *Physical Review Letters*, **80**:684–687, 1998.

[76] C. H. Greene. **Photoabsorption Spectra of the Heavy Alkali-Metal Negative Ions**. *Physical Review A*, **42**:1405–1415, 1990.

[77] C. F. Fischer and D. Chen. **Numerical Multiconfiguration Hartree-Fock Calculations for nsnp ^{3}P States of Rb and Cs Negative Ions**. *Journal of Molecular Structure: THEOCHEM*, **199**:61–73, 1989.

[78] C. Bahrim, U. Thumm, A. Khuskivadze, and I. I. Fabrikant. **Near-Threshold Photodetachment of Heavy Alkali-Metal Anions**. *Physical Review A*, **66**:052712, 2002.

[79] H. Friedrich. *Theorethical Atomic Physics*. Springer, Berlin, 1991.

[80] J. Sandström, G. Haeffler, I. Kiyan, U. Berzinsh, D. Hanstorp, D. J. Pegg, J. C. Hunnell, and S. J. Ward. **Effect of polarization on photodetachment thresholds**. *Physical Review A*, **70**:052707, 2004.

[81] W. A. van Wijngaarden and J Li. **Polarizabilities of Cesium S, P, D, and F States**. *Journal of Quantitative Spectroscopy & Radiative Transfer*, **52**:555–562, 1994.

[82] C. Blondel, P. Cacciani, C. Delsart, and R. Trainham. **High-Resolution Determination of the Electron Affinity of Fluorine and Bromine Using Crossed Ion and Laser Beams**. *Physical Review A*, **40**:3698–3702, 1989.

[83] M. Scheer, C. A. Brodie, R. C. Bilodeau, and H. K. Haugen. **Laser Spectroscopic Measurements of Binding Energies and Fine-Structure Splittings of Co^-, Ni^-, Rh^-, and Pd^-**. *Physical Review A*, **58**:2051–2062, 1998.

[84] S. Watanabe and C. H. Greene. **Atomic Polarizability in Negative-Ion Photodetachment**. *Physical Review A*, **22**:158–169, 1980.

[85] A. A. Radzig and B. M. Smirnov. *Reference Data on Atoms, Molecules and Ions*. Springer-Verlag, Berlin, 1985.

[86] H. Hotop and W. C. Lineberger. **Binding Energies in Atomic Negative Ions: II**. *Journal of Physical and Chemical Reference Data*, **14**:731–750, 1985.

[87] K. H. Weber and C. J. Sansonetti. **Accurate Energies of nS, nP, nD, nF, and nG Levels of Neutral Cesium**. *Physical Review A*, **35**:4650–4660, 1987.

[88] A. Kellerbauer and S. Fritzsche. **High-Resolution Optical Spectroscopy of Os^- With a View to Laser Cooling of Atomic Anions**. *Journal of Physics: Conference Series*, **388**:012023, 2012.

[89] S. O'Malley and D. R. Beck. **Valence Calculations of Lanthanide Anion Binding Energies: 6p and 6s Attachments to $4f^m(5d + 6s + 6p)^3$ Thresholds**. *Physical Review A*, **79**:012511, 2009.

[90] A. M. Covington, D. Calabrese, J. S. Thompson, and T. J. Kvale. **Measurement of the Electron Affinity of Lanthanum**. *Journal of Physics B: Atomic and Molecular Physics*, **31**:L855–L860, 1998.

[91] M. Blatt and V. F. Weisskopf. *Theorethical Nuclear Physics*. Springer-Verlag, New York, 1979.

[92] E. Werner. *The Distribution and Correlations of a Polymer Confined to a Channel*. Licentiate thesis, University of Gothenburg, 2013.